INVITED PAPER

Optical Biosensors Based on Plasmonic Nanostructures: A Review

This paper reviews the fundamentals of optical biosensors and presents recent technological advances and applications.

By Barbora Špačková, Piotr Wrobel, Markéta Bocková, Jiří Homola

ABSTRACT | This paper reviews fundamentals of optical affinity biosensors based on plasmonic nanostructures and discusses recent advances in the development of this technology, including plasmonic nanostructures and surface plasmon phenomena, advances in sensor instrumentation, and functional coatings. Examples of applications for both the detection of chemical and biological substances as well as the investigation of biomolecular interactions are also given.

KEYWORDS | Biomolecular interaction analysis; detection of biomolecules; functional coating; metal nanostructure; microfluidics; optical biosensor; plasmonics; refractive index sensing; surface plasmon

I. INTRODUCTION

Although plasmonic phenomena have been known for more than a century, their potential for molecular sensing was not recognized for many years, a stay that lasted until the 1970s and 1980s. In the 1970s, an unexpected enhancement of Raman scattering near a roughened metal surface was observed by Fleischmann *et al.* [11] and later associated with an electromagnetic effect by Jeanmaire and Van Duyne [17]. This enhancement was initially described in terms of electromagnetic modes, which are now referred to as localized surface plasmons (LSPs). In the 1980s, another kind of surface plasmon (SP), the so-called propagating surface plasmon (PSP), was exploited by Liedberg *et al.* to detect a refractive index (RI) change caused by the adsorption of molecules onto a surface of a metal film [23]. In the following decades, refractometric biosensors exploiting PSPs [sometimes referred to as surface plasmon resonance (SPR) sensors] have made great advances both in terms of technology and applications [12]. By enabling real-time investigation of biomolecular interactions, SPR biosensors have become an important tool in molecular biology. In addition, SPR biosensors have been demonstrated to hold vast potential for rapid label-free detection of chemical and biological species in numerous fields, including medical diagnostics, environmental monitoring, and food safety and security [34]. Recent advances in technologies for the fabrication (electron-beam and ion-beam lithography) and characterization (scanning electron and atomic force microscopy) of plasmonic nanostructures [36]–[40] have catalyzed the rapid development of the field of nanoplasmonics [42], [43], and in turn, the discovery of numerous novel plasmonic phenomena. These advances have opened the doors to novel sensing concepts and applications. Optical biosensors based on plasmonic nanostructures have become subject of extensive research and have been featured in numerous books [44]–[46] and reviews [48]–[58].

This paper presents the fundamentals of optical affinity biosensors based on plasmonic nanostructures and, furthermore, reviews advances in the development of plasmonic biosensors since 2009. Specifically, this review covers plasmonic nanostructures and surface plasmon phenomena, optical platforms for excitation and interrogation of SPs, and functional coatings for affinity-based biosensing. Applications of optical biosensors based on plasmonic nanostructures for both the detection of chemical and biological substances as well as the investigation of biomolecular interactions are also reviewed. It should be noted that sensors based on PSPs on continuous metal films and sensors based on plasmonic nanoparticles in solution are outside the scope of this review; however, there are a number of recent reviews on these topics [60]– [66], to which we refer the reader.

Manuscript received August 14, 2016; revised October 28, 2016; accepted October 29, 2016. Date of current version November 18, 2016. This work was supported by the Czech Science Foundation under Contract P205/12/G118 and by Praemium Academiae of the Czech Academy of Sciences.
The authors are with the Institute of Photonics and Electronics AS CR, v. v. i, Prague, 182 51, Czech Republic (e-mail: homola@ufe.cz).

Digital Object Identifier: 10.1109/JPROC.2016.2624340

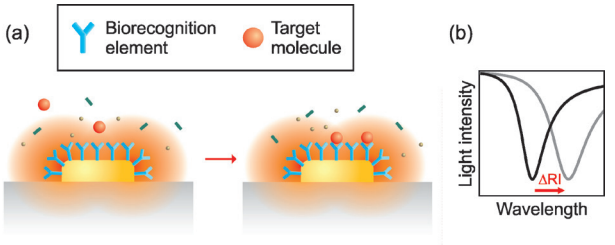

Fig. 1. ***(a) Principle of a plasmonic affinity biosensor. (b) Change in the spectrum due to the increase of RI in the proximity of a sensor surface induced by captured target molecules.***

II. PRINCIPLES OF PLASMONIC BIOSENSING

Plasmonic affinity biosensors belong to the group of optical label-free affinity biosensors. In general, plasmonic affinity biosensors are composed of sensing elements that comprise metal or metal–dielectric nanostructures supporting SPs and biorecognition elements (receptors) that are able to selectively bind a target molecule (analyte). Illumination of the sensing element by light generates SPs on the nanostructures producing the EM field that is highly concentrated at the surface of the nanostructures. When a solution containing analyte molecules is brought into contact with the biosensor, the capture of analyte by receptor immobilized on the surface of the sensing element gives rise to a change in the RI in the region close to the surface [Fig. 1(a)]. As the characteristics of an SP are very sensitive to changes in the RI in the proximity of the surface, changes in the local RI induced by the binding of analyte can be determined by measuring changes in one of the characteristics of the light coupled to SP, for example, changes in the resonant wavelength, intensity, or phase [Fig. 1(b)].

The most common nanostructure used in plasmonic biosensing is a metal nanoparticle (NP) supporting an LSP on a dielectric substrate. The excitation of a LSP by a light wave is associated with the strong absorption and scattering of the light and furthermore, a high enhancement of an electromagnetic (EM) field in the vicinity of the NP [72]. The wavelength at which the excitation of an LSP takes place depends on the shape, size, and composition of the NP and, for most noble metals, lies in the visible or near-infrared region of the electromagnetic spectrum. While metal NPs having a spherical shape exhibit LSPs at shorter wavelengths of the visible spectra [Fig. 2(a)], LSPs at longer wavelengths can be excited by core-shell NPs [76] or nanorings [79], NPs having a high aspect ratio [e.g., nanorods, Fig. 2(b)] [84], and NPs with sharp edges (e.g., nanoprisms [89] or nanostars [92]). In addition, complex nanostructures have recently been proposed that exhibit LSPs at infrared region [93]–[96].

The EM field surrounding a metal NP decays with the distance (z) from the surface of the NP according to $1/z^3$ [100]. Nonetheless, the approximation of exponential decay is widely used [105] and the penetration of the EM field into the medium is often expressed in terms of a decay length, defined as the distance from the interface at which the amplitude of the field decreases by a factor of $1/e$. The decay length of LSPs excited on metal NPs in the visible or near-infrared wavelengths is dependent on both the resonant wavelength and the parameters of the NP [107], but is typically comparable to the size of an NP. Decay lengths on the order of hundreds of nanometers have been reported for complex nanostructures with resonances in the infrared spectral region [96], [109], [110]. In addition to NPs, a single nanohole in a metal layer has also been shown to be able to support an LSP [111].

An interesting situation arises when two metal NPs (supporting LSPs) are in close proximity with one another, whereby the interaction of their EM fields can give rise to coupled SP modes [112] [Fig. 2(c)]. Due to strong charge buildup, the EM field becomes squeezed in the gap between the two NPs, which results in a significant field enhancement. This highly localized and enhanced EM field makes a variety of plasmonic nanostructures attractive for biosensing, including NP dimers [114], "bow-ties" [116], and NP aggregates [118].

Recently, structures supporting Fano resonances, such as nanoparticle oligomers [119], [120] or nanohole oligomers [80], [121], ring-disk nanocavities [123], and nanocubes placed on high RI substrate [126] have received a great deal of attention. Fano resonances originate from the interference between light directly coupled to a bright mode and light indirectly coupled to a dark mode excited via near-field interactions with the bright mode [127], [128]. Narrow dips in the spectrum arise as the two modes interfere destructively as the dark mode is out of phase with respect to the bright mode [Fig. 2(d)].

Metal NPs arranged into a periodic array can support resonances which originates from coupling of LSP and the Rayleigh anomalies (RAs), sometimes referred to as surface lattice resonances (SLRs) [130], [131]. In contrast to LSP, SLR is associated with an EM field that is rather delocalized and its excitation is manifested by considerably narrower spectral features [Fig. 2(f)]. The wavelength at which SLRs are excited can be tuned by varying the period, angle of incidence, and geometric parameters of the NPs [131]–[133].

Random arrays of metal NPs on a dielectric substrate have also been demonstrated to support guided modes of EM fields, similar to the modes supported by thin absorbing films [108].

Finally, metal nanostructures can also support complex modes that arise from the coupling of LSP and PSP. Although PSPs [sometimes referred to as surface plasmon polaritons (SPPs)] are typically excited by attenuated total reflection or diffraction couplers on continuous metal films [12], periodic nanostructures may provide an alternative coupling mechanism, giving rise to coupled LSP–PSP modes sometimes referred to as SPP–Bloch waves [138] [Fig. 2(e)]. In comparison with an LSP, the EM field of a PSP is more delocalized and its decay length is typically in the orders of hundreds of nanometers [12].

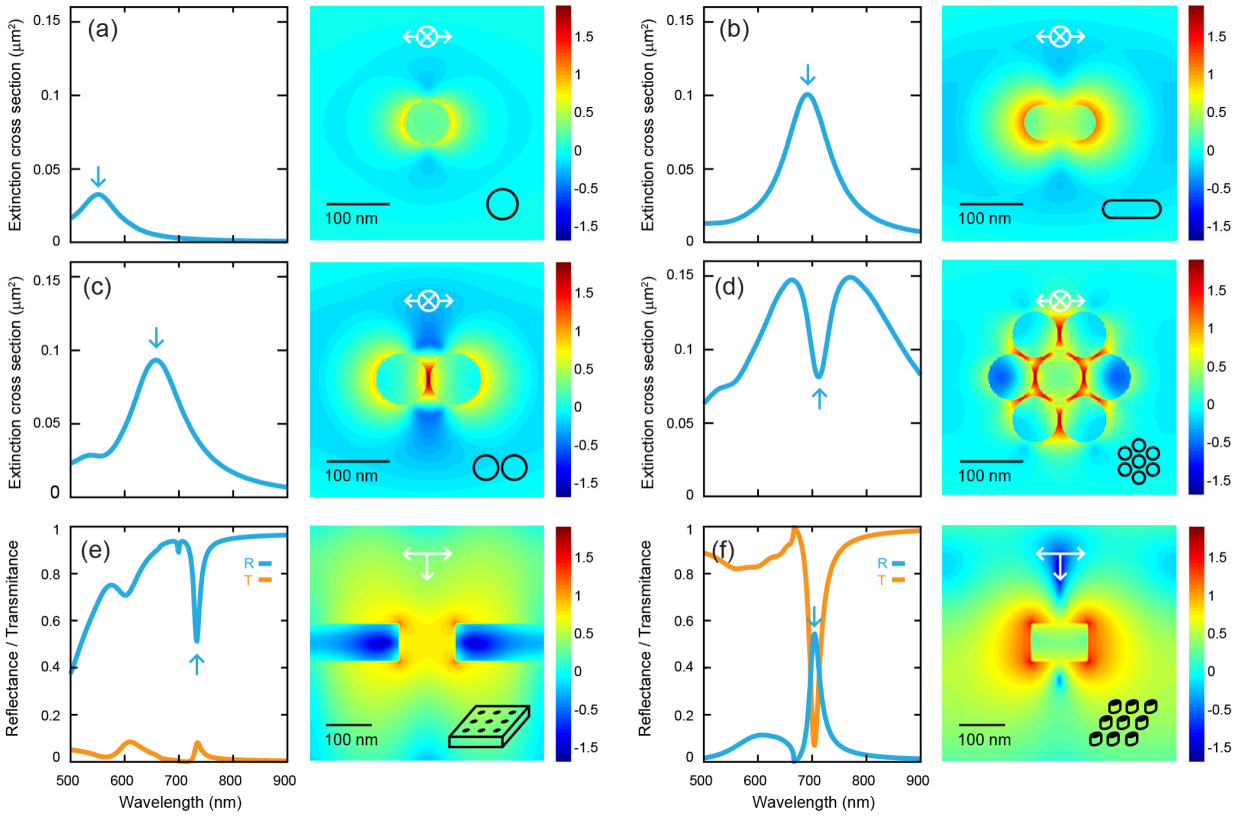

Fig. 2. ***Spectral characteristics and electric field distributions |E| at the resonant wavelength of typical plasmonic substrates used in biosensing. (a) Au sphere with diameter 80 nm. (b) Au nanorod with diameter 80 nm and length 120 nm. (c) Dimer of Au spheres with diameter 80 nm and separation distance 5 nm. (d) Heptamer of Au spheres with diameter 80 nm and separation distance 5 nm. (e) Periodic arrays of nanoholes with diameter 120 nm in Au film with thickness 80 nm. (f) Periodic arrays of Au nanodisks with diameter 120 nm and height 80 nm. Structures are surrounded by a symmetric environment having a RI of water (1.33). These characteristics were calculated using FDTD (Lumerical). The colorbar is in the logarithmic scale.***

The decay length of coupled LSP–PSP modes thus depends on the relative strength of each mode and can be tuned by the design of the nanostructure; for example, plasmonic modes on nanohole arrays exhibit larger decay lengths with respect to those on NP arrays due to the excitation of LSP–PSP coupled modes in the former [140]. Periodic arrays of nanoholes have been extensively explored in the context of extraordinary optical transmission (EOT) [142]. Apart from SPP–Bloch waves, this structure can support RA–SPPs which have common origins with SLRs excited on NP arrays [131], [144].

It is clear that the full richness of physical phenomena would not be experimentally accessible without the major advances in nanofabrication that took place in the last two decades. The current portfolio of methods used for the fabrication of nanostructures for plasmonic biosensors encompasses a broad range of methods, including complex and versatile methods allowing precise fabrication of extremely small features, such as electron–beam and ion–beam lithography, methods enabling cost-effective fabrication of nanostructures over large areas, such as interference or colloidal lithography, and simple methods for production of metal nanoparticles based on wet chemical reduction or vapor deposition techniques. It is not the aim of this paper to review these methods. Instead, we refer the reader to specialized review articles that provide in-depth coverage of this important area [36], [145]–[147].

III. PERFORMANCE CHARACTERISTICS OF PLASMONIC BIOSENSORS

The performance characteristics of a biosensor can be defined in several manners. In the context of sensing, however, the most important characteristics are related to the ability of a sensor to detect an analyte present in solution. In this section, we define and discuss several performance characteristics related to biosensors based on plasmonic nanostructures. It should be noted that although SPR sensors based on PSPs are outside the scope of this review, their performance serves as a reference for comparison to the nanoplasmonic biosensors discussed herein.

Table 1 Examples of Plasmonic Nanostructures Used in Sensing Along With Their Bulk Refractive Index Sensitivity (S_B) and Figure of Merit (FOM_B)

Phenomenon	Nanostructure	Type of study	Resonant wavelength	S_B [nm/RIU]	FOM_B [1/RIU]	Ref.
PSP	Planar Au layer (excited in ATR configuration)	Theory	600 – 1000	1000 – 14000	20 - 140	[4]
	Gold diffraction grating	Theory	600 – 1000	300 – 700	-	[12]
	Planar Au layer is symmetric media (Long-range PSPR)	Theory	550 - 850	500 – 200000	-	[12]
LSP	Au nanorod	Theory	600 – 1000	200 – 600	4 - 10	[4]
	Edge Au-coated Ag nanoprisms	Exp.	600	425	3	[26]
	Au nanoprisms	Exp.	626, 700	583, 647	4.9, 5.1	[27, 28]
	Au nanostar	Exp.	650 – 750	218	5	[33]
	Au nanoring	Exp.	870	350	3.1	[59]
	Au bipyramids	Exp.	900	381	3.8	[67]
	Au nanocross	Exp.	1400	500	2	[70]
Fano resonance	Au dolmen	Theory	770	435	42	[8]
	Au NP heptamer	Theory	650	-	9.3	[8]
	Au nanohole quadrumer	Theory	680	338	14.25	[80]
	Au nanopillar	Exp.	1300 – 1500	300 – 1000	10 - 16	[85]
LSP-PSP coupled mode	Periodic nanopillars on Au layer	Exp.	815	675	112.5	[87]
	Periodic array of Au mushrooms	Exp.	1260	1010	108	[90]
	Nanoholes array in Au film	Exp.	660 - 750	360 – 480	-	[97]
SLR	Periodic arrays of Au nanodisks	Exp.	600 – 900	-	0.6 – 25	[99]
	Periodic arrays of Au ellipsoids	Theory	500 – 1000	-	300 – 4 000	[103]
	Suspended nanoholes array in Au film	Exp.	795	717	162	[104]
Guided mode	Au nanorod layer	Exp.	1280	32000	330	[108]

A. Bulk Refractive Index Sensitivity and Figure of Merit

The most widely used performance characteristic of a plasmonic sensor lies in the ability to detect changes in the RI. This is often quantified as the bulk RI sensitivity (S_B), defined as

$$S_B = \frac{d\lambda_r}{dn_B} \tag{1}$$

where λ_r is the wavelength at which the excitation of an SP occurs (resonant wavelength) and n_B is the RI of the medium in the contact with the sensor surface. Typical S_B values for a variety of plasmonic nanostructures, measured both theoretically and experimentally, are shown in Table 1. It can be seen that the values of S_B have substantial variability, and among other parameters, depend on the type of the supporting EM mode (decay length), resonant wavelength, excitation geometry, and properties of the substrate. These factors are discussed below.

One of the main factors that affect S_B is the level of localization of the EM mode. As seen in Table 1, substantially higher values of S_B are reported for delocalized modes with respect to those for localized modes. Maximum values of S_B that can be obtained using PSPs excited on a gold film can exceed the S_B of an LSP on a gold NP by more than an order of magnitude [4]; when compared to long-range PSPs on a continuous gold film that difference can be two orders of magnitude [12]. Comparably high S_B has also been achieved using a guided mode supported by a nanorod array [108]. A number of nanostructures enabling efficient LSP–PSP coupling (e.g., periodic arrays of nanoholes or other nanoscopic features on a continuous metal layer) have been reported to provide S_B values between those obtained from sole LSP and PSP modes. In these applications, the S_B value is dependent on the coupling strength between the two modes [153]. A strong correlation between S_B and the decay length was demonstrated for both LSP excited on NPs of different sizes and shapes [107] as well as SLRs excited on periodic arrays of NPs (with varying strength of the LSP–SLR coupling) [154], [155].

The dependence of S_B on geometrical parameters of an NP surrounded by a (homogeneous) sample has been investigated by several groups [4], [27], [67], [156]–[158]. A theoretical analysis has shown that S_B depends on the optical constants of the metal and increases with the resonant wavelength, regardless of the shape of the NP [156], [157]. Bulk refractive index sensitivity of sensors based on LSPs excited on surface bound metal NPs (on a dielectric substrate) are typically lower with respect to the sensitivity of metal NPs surrounded by a homogeneous sample. Nonetheless, for most NP shapes, S_B of sensors employing NPs on dielectric substrates also increases with the resonant wavelength. This has been demonstrated for several NPs, whereby changes to the resonant wavelength were varied with changes in the NP size [67], aspect ratio [4], or sharpness of edges [158]. An opposite trend (decreasing S_B with increasing resonant wavelength) has been only reported concerning nanoprisms of different sizes, where the influence of the substrate was shown to be strong enough to disrupt the observed trend for nanoprisms surrounded by a homogeneous medium [27]. The influence of the substrate on S_B of NPs (silver nanocube) was investigated theoretically by Mahmoud *et al.* [159]. They showed that the presence of a higher RI substrate under an NP breaks the symmetry of the EM near-field around the NP, where a large portion of the EM field is shifted to the substrate, thus becoming unavailable for sensing. In order to distribute the EM field in a more symmetric

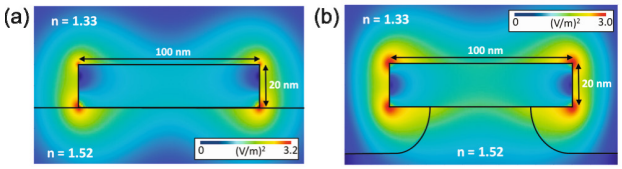

Fig. 3. *(a) Near-field electric field profile of a single gold nanodisk located on a supporting substrate (n = 1.52) and surrounded by a homogeneous dielectric medium (n = 1.33). (b) Near-field electromagnetic field profile of a suspended single gold nanodisk supported by a 22-nm isotropic pillar (n = 1.52) and surrounded by a dielectric medium (n = 1.33). Adapted with permission from [6]. Copyright 2011 ACS Publication.*

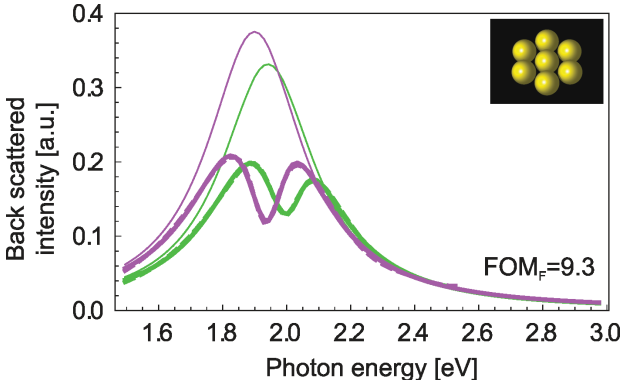

Fig. 4. *FOM$_F$ of an isolated gold heptamer. FOM$_F$ takes into account the sensitivity, the spectral resolution, and the contrast of the Fano line shape. The spheres' radius is 30 nm, and their center-to-center distance is 65 nm. The green and purple lines refer to a surrounding refractive index of 1.33 and 1.40, respectively. The thick solid line refers to the calculated backscattered light intensity, the dashed line to the fit with the Fano resonance formula, and the thin solid line to the extracted Lorentzian envelope. Adapted with permission from [8]. Copyright 2013 ACS Publication.*

manner and thus increase the sensitivity, the use of a low refractive index substrate was proposed [160]. An alternative approach to increase S_B—based on increasing the availability of the EM field around an NP—has been proposed in which the "bottom" side of an NP was exposed to the surround medium using suspended NPs on dielectric pillars (Fig. 3) [6], [161].

It has also been shown that S_B of LSP-based sensors can be influenced by the excitation geometry. Kedem *et al.* demonstrated that the sensitivity of the spectral peak corresponding to LSPs excited on an array of gold NPs may be higher by a factor of 2 when observed in the reflectance spectrum (with respect to transmittance) [162], [163]. Špačková *et al.* observed abnormal behavior of S_B of a sensor based on an array of gold NPs on a glass substrate illuminated in the ATR geometry. In this study, S_B was shown to be dependent on the angle of incidence (pertaining to the illumination of the NP array), with the variation of S_B spanning between positive and negative values [164].

The ability of a plasmonic sensor to measure minute changes in the RI is directly proportional to S_B and, furthermore, inversely proportional to the width w of the resonant feature (spectral dip or peak) being tracked. The combination of these parameters is often referred to as the figure of merit

$$\mathrm{FOM}_B = \frac{S_B}{w} \tag{2}$$

which is widely used, as it allows for the evaluation and comparison of different plasmonic nanostructures with respect to their sensing potential.

Values of FOM_B reported for a number of plasmonic nanostructures are shown in Table 1. It can be seen that LSP-based sensors offer FOM_B values that are about one order of magnitude lower than those provided by PSP-based sensors. The FOM_B of LSP-based sensors are dependent on the resonant wavelength and can exhibit a local maximum; for example, gold nanorods of variable aspect ratio were shown to exhibit a maximum value of FOM_B when the LSP was excited at a wavelength of around 700 nm [4], [165]. Higher FOM_B values have been achieved using more delocalized modes that produce narrower spectral features, such as LSP–PSP coupled modes exited via diffractive coupling in plasmonic crystals [87] or SLRs excited on periodic array of NPs [90], [99].

An approach to improve FOM_B by reducing the spectral width of a plasmonic feature is based on the use of Fano resonances [8], [80], [85], [94], [121], [126], [166], [167]. As shown by Gallinet and Martin [8], Fano-resonant systems may potentially exceed the more conventional Lorentz-resonant systems in terms of FOM_B; however, the limited contrast of plasmonic spectral features can limit the systems to translate improvements in FOM_B to an ability to detect smaller changes in the bulk RI (Fig. 4).

B. Refractive Index Resolution

The RI resolution of a plasmonic sensor is defined as the smallest change in the RI that produces a detectable change in the sensor output, and it is widely used to characterize the experimental performance of plasmonic sensors. It is typically expressed in terms of the standard deviation of noise of the sensor output σ_{SO} and bulk sensitivity S_B [34]

$$\sigma_{\mathrm{RI}} = \frac{\sigma_{SO}}{S_B}. \tag{3}$$

Refractive index resolution is a compound characteristics determined by the parameters of a plasmonic nanostructure and characteristics of an optical platform used to excite an SP mode on the nanostructure (more details in Section IV).

C. Surface Refractive Index Sensitivity and Figure of Merit

In plasmonic affinity biosensors, the capture of analyte does not (usually) take place over the entire volume corresponding to the EM field of the plasmonic mode, but rather at the vicinity of the metal surface to which receptors are attached. Because the binding-induced changes to the RI are limited to a finite distance from the surface, a performance characteristic describing the response of a plasmonic sensor to surface RI changes is highly relevant.

The surface RI sensitivity S_S is usually defined as the sensitivity to RI changes confined in a thin layer and can be written as

$$S_S = \frac{d\lambda_r}{dn_s}. \quad (4)$$

As shown by several studies, the local sensitivity to RI changes is highly correlated with both spatial distribution of an EM field [168], [169] and the strength of a plasmonic mode within the confined layer (Fig. 5) [170]. Assuming the exponential decay of the EM field, S_S can be expressed in terms of S_B, the decay length of the EM field l_d, the thickness h of the layer where RI changes take place, and the distance h_0 of the layer from the metal surface [170]

$$S_S \approx S_B \exp(-2h_0/l_d)\left[1 - \exp(-2h/l_d)\right]. \quad (5)$$

Interestingly, several studies have reported that the spectral position of the extinction maximum of metal NPs responds to dielectric overlayers having thicknesses that extend far beyond the decay length of the respective LSP [171], [172]. This has since been attributed to either a superposition of the plasmon spectra with thin-film interference [173], [174] or to an increase of the scattering coefficient associated with an increase of the NP size [175].

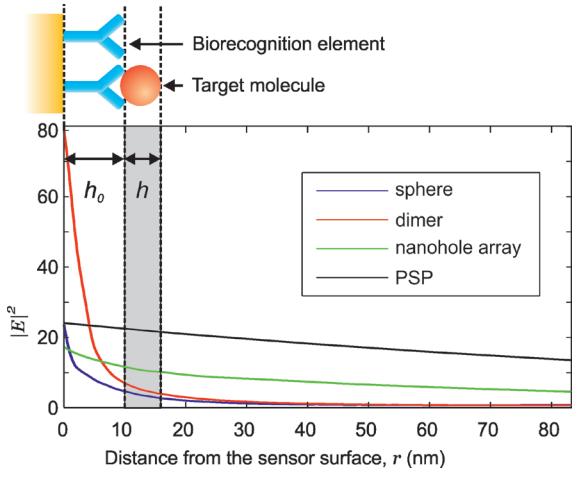

Fig. 5. ***The dependence of the electric field on the distance from the metal surface (area averaged) in the dielectric medium associated with resonances excited on different kinds of plasmonic structures. The parameters of the nanostructures were taken from Fig. 2, and the PSP resonant wavelength was set to 750 nm.***

Similar to the definition of FOM_B, the figure of merit for surface refractive index changes FOM_S can be defined as

$$\mathrm{FOM}_S = \frac{S_S}{w} \approx \mathrm{FOM}_B \exp(-2h_0/l_d)\left[1 - \exp(-2h/l_d)\right]. \quad (6)$$

The optimization of a plasmonic nanostructure in terms of FOM_S is a complex task, where one must consider not only FOM_B, but also both the dimensions of the target analyte and the EM field distribution of the plasmonic mode.

While structures offering rather short decay lengths (LSP-based structures) may be efficient for the detection of small or medium-size molecules, nanostructures with longer decay lengths may be preferred for the detection of either large analytes, such as viruses or bacteria, or for the detection of binding events that do not take place directly on the metal surface (e.g., when a relatively thick functional biolayer is used). This duality has recently been described in the work of Mazzotta *et al.*, who showed that due to the longer decay length of nanoholes compared to nanodisks (due to the coupling to PSPs), nanodisks outperform (in terms of S_S) nanoholes for surface RI changes confined more tightly to the surface ($< \sim$20 nm), while the opposite holds true for refractive index changes that are less confined ($> \sim$20 nm) [140].

Due to the lack of standards for both the experimental and theoretical determination of both S_S and FOM_S, it is difficult to make a meaningful comparison of the theoretical and experimental data recently published by different research groups; however, there are a few exceptions to this general trend. Simulations of both LSPs excited on ellipsoidal NPs and PSPs excited on continuous metal layer have shown that, upon parameter optimization of each system, both can exhibit similar FOM_S values (surface RI changes were simulated to occur within an infinitesimally thin layer) [4]. In another theoretical work, FOM_S was compared for LSPs and SLRs excited on arrays of general ellipsoids (in this study, surface RI changes were assumed to occur within the distance of 10 nm away from the metal surface). This study predicted comparable FOM_S for optimized parameters of the two structures, albeit FOM_B calculated for the SLRs was two orders of magnitude higher than that for the LSPs [103]. An experimental comparison of the responses of PSP- and LSP-based sensors to biotin–avidin coupling was performed by Svedendahl *et al.*, who demonstrated that the two approaches exhibit a comparable S_S under identical experimental conditions [176].

D. Limit of Detection, Molecular Detection Limit

The ability of an affinity biosensor to detect molecular analyte captured onto the sensor surface can be characterized by the surface coverage resolution σ_Γ, which is defined as the minimum resolvable change in the mass of captured molecules (per surface area) and can be expressed as

$$\sigma_\Gamma = \frac{\sigma_{SO}}{S_\Gamma} \quad (7)$$

where S_Γ denotes the sensitivity to molecular mass surface coverage. While σ_Γ of biosensors based on continuous metal films is mainly defined by σ_{RI} ($\sigma_{RI} = 10^{-7}$ RIU corresponds to $\sigma_\Gamma = 91$ fg/mm^2 [34]), σ_Γ of a biosensor based on nanostructured substrate can be improved due to decreased sensing area ($\sigma_\Gamma = 35$ fg/mm^2 was reported for biodetection on array of nanorods [177]). Recently, several groups have suggested a route to significant improvement of σ_Γ by localizing biomolecular interactions exclusively to the regions having enhanced EM fields [178]–[183].

While σ_Γ characterizes the ability of a sensor to detect minute amounts of analyte molecules on the sensor surface, it does not address the topic of analyte transport from the bulk volume (of the sample solution) to the surface of the sensor, and thus does not sufficiently provide all analytically relevant information.

The bioanalytical power of a biosensor is best described by the limit of detection (LOD). The LOD (typically expressed in units of concentration) describes the smallest concentration (or amount) of analyte that can be reliably detected by a specific measurement process (IUPAC Definition). It is usually defined as the concentration of analyte that produces a sensor response corresponding to three standard deviations of the sensor response measured for a blank sample σ_b (sample with no analyte) and can be expressed as

$$\mathrm{LOD} = \frac{3\sigma_b}{S_c} \tag{8}$$

where S_c is the change in the sensor output divided by the change in the concentration of analyte producing it and it depends on S_Γ, the rate of mass transport to the sensor surface and the kinetic parameters of the interaction between analyte and biorecognition element. Reported values of LOD varied substantially across the applications, and the examples are given and discussed in more details in Section VII.

Advances in plasmonic nanostructures and ability to create highly localized EM fields in volumes comparable to that of an individual molecule, such as proteins or nucleic acids, have encouraged researchers to expand plasmonic nanostructures toward the investigation of processes involving a small number of (or even individual) biomolecules. The characterization of the ability of a plasmonic biosensor to detect individual molecules has been recently introduced as the molecular detection limit (MDL): the smallest number of bound molecules that is measurable by a sensor. It follows that the MLD depends on the characteristics of a plasmonic nanostructure (S_B, distribution of the EM field), optical platform, and characteristic sizes of receptor and analyte [184], [185].

Using nanostructures having hot spots generated at the edge or the tips, several papers have reported on the detection with MDLs at the single molecule level, including the detection of a relatively large protein (fibronectin) on a gold nanorod [186], the detection of a medium-size protein (streptavidin) on a gold nanorod [187], and the detection of an antigen–antibody pair using bipyramids [188].

IV. OPTICAL PLATFORMS

A plasmonic nanostructure must be combined with an optical platform in order to realize its potential for biosensing purposes; these optical platforms aid to couple light to a plasmon mode, thereby transferring biomolecular information (e.g., concentration of analyte) to the output light, which is then converted to a sensor output. The optical platform is thus an important functional component of a plasmonic biosensor and its properties have direct impact on the biosensor performance characteristics, such as sensitivity or limit of detection. As expected, there is currently a wide range of platforms used with plasmonic nanostructures, with differences in complexity, performance, and targeted application field. In this section, we review the main configurations of optical platforms utilized with plasmonic nanostructures and present several recent advancements in their development.

A. Configurations of Optical Platforms

For plasmonic biosensors based on arrays of metal NPs, the most straightforward optical arrangement relies on the excitation of surface plasmon modes by normally incident light in a collinear arrangement of the light source module, plasmonic nanostructure, and detector module: this arrangement is used in either transmission [143], [189] or reflection mode [162]. While the transmission mode enables greater simplification of the optical platform, the reflection mode may be preferred in situations when either highly absorbing or scattering samples are to be analyzed [190] or the plasmonic nanostructure needs to be interfaced with complex microfluidics and/or temperature stabilizations. Unlike optical systems used in conventional SPR sensors that employ prism couplers to excite PSPs on continuous metal films, this collinear arrangement does not require any coupling optics and thus enables the construction of simpler, more compact, and potentially more cost-effective optical platforms [1], [191]–[193]. It should be noted, however, that optical designs driven by requirements for high degree of miniaturization and cost reductions may results in platform with a lower performance when compared to high-performance optical systems [20].

Another optical configuration that has been employed with plasmonic biosensors is based on the attenuated total reflection (ATR) geometry. In this configuration, light is coupled to a plasmonic nanostructure placed on the base of a prism via an evanescent field generated when the light is made incident on the base of the prism under an angle of incidence larger than the critical angle. ATR configurations have been used in conjunction with plasmonic nanostructures supporting both Fano resonances [164] and

waveguide modes [108]. It should be also noted that in the ATR configuration, the operational conditions can be optimized by tuning the angle of incidence (thus also tuning the propagation constant of the evanescent wave); for example, to achieve coupling between localized and propagating plasmons excited on arrays of nanoholes [194], or to reach near-zero reflection in phase sensitive measurements [195]. Moreover, ATR configurations have been shown to enable background noise suppression in scattering spectroscopy [117].

Configurations based on optical microscopy are used when plasmonic modes are to be excited or interrogated on limited areas of plasmonic nanostructures (or individual NPs) to either observe events involving a small number of molecules [196], [197] or likewise, to avoid ensemble averaging in nonuniform structures (which cause broadening of spectral features) [33]; both transmission and reflection modes can be utilized in microscopic configurations. In addition, this optical configuration makes it possible to perform spectroscopic analysis and imaging simultaneously [198], [199]. When the readout from extremely small areas is desired, such as from a single NP, the signal-to-noise ratio (SNR) becomes strongly affected by background light; in such cases, optical configurations allowing for efficient suppression of background noise need to be employed. One commonly used approach is dark-field microscopy (DFM), in which a condenser with a central stop and an objective with a small numerical aperture are used to collect only the light scattered by an NP [200]. Due to low light levels, the increased contrast obtained by DFM comes at a price of higher noise in comparison with extinction measurements using a conventional microscope [196]. Another challenge for DFM measurements is the noise originating from mechanical instabilities, which are increasingly pronounced with reductions in the readout area. Both noise types limit the accuracy of DFM optical configurations, whereby longer integration times and signal averaging are required. Using the DFM approach, Mayer *et al.* monitored the scattering spectra of individual gold nanopyramids to detect single molecule events; due to a low temporal resolution, they were able to detect only slow unbinding events [188].

Several alternative approaches to conventional DFM have been recently proposed for optical system simplification and furthermore, to increase the contrast of collected images in microscopy system. One approach takes advantage of metal NPs placed on a perforated chromium layer having nanoholes with a size comparable to the NP diameter [201]. This arrangement leads to increased scattering from NPs and, though collecting only the light transmitted through the holes, a suppression of the background noise. To improve both the temporal resolution and the SNR, Ament *et al.* proposed to use a standard upright microscope with ATR illumination [186]. In combination with a high power (2.8 W) white light source, a nanorod array optimized to yield the highest scattered signal, and an intensified charge-coupled device (CCD) camera, their optical configuration allowed for the observation of single protein binding events with a millisecond temporal resolution. A simplification of ATR illumination was also proposed by Chamanzar *et al.*, who used an on-chip photonic waveguide to measure the scattering of light from either single or chains of Au nanorods integrated with the waveguide [202].

Another optical configuration is based on metal nanoparticles (or nanostructures) integrated onto an optical waveguide, typically in the form of an optical fiber. In contrast to microscopy, optical fibers offer a simple and robust optical platform that can be readily combined with compact fiber optic spectrometers and light sources [203], [204]. In addition, fiber optic sensors offer numerous other advantages, including a high degree of miniaturization, potential for remote sensing, and highly localized measurements. Commonly used schemes are based on nanoparticles attached either on the tip [205]–[207] or along a stripped part of a straight [208], [209] or bent [35], [210] optical fiber. Schemes with NPs attached along an optical fiber are usually operated in transmission mode [32]. When NPs or a plasmonic nanostructure is placed on a tip of a fiber, the sensor can operate either in transmission mode [211], [212] or in the reflection mode, whereby an optical fiber coupler [206] or a beam splitter [149], [213] is used to connect the light source and the spectrometer. Multiple fibers arranged in a fiber bundle have been demonstrated to allow for multiplexed measurements [211]. In comparison to a conventional fiber-optic SPR sensor employing PSPs propagating along continuous metal films, NP-based fiber optic sensors have a lower sensitivity to interferences causing fluctuations in polarization of light guided by the fiber, and thus have better stability and resolution [214]. Finally, optical platforms based on planar waveguides that are fabricated by already mature technologies and allow for high degree of miniaturization should be also mentioned. The use of planar waveguides was advocated by Ozhikandathil and Packirisamy who reported on an optical configuration based on an array of Au nano-islands on the top of a silica-on-silicon (SOS) waveguide [215].

B. Interrogation Methods

The optical configuration of a plasmonic biosensor is in a large part determined by the methods used to generate the biosensor output, namely, what characteristic of light is interrogated. Plasmonic biosensors can thus be classified into those that use wavelength, intensity, and phase interrogation methods. In this section, we give examples of typical implementations for each interrogation method, showing the strengths and weaknesses of each, furthermore illustrating the trends in their development.

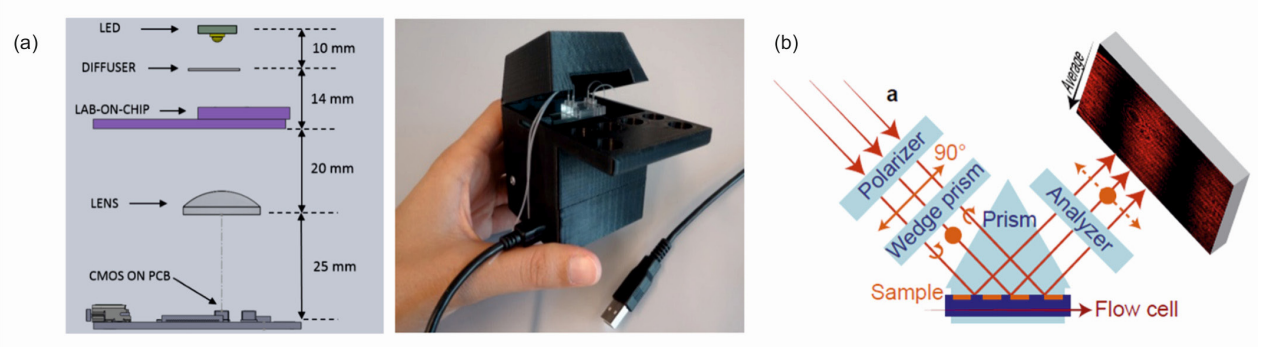

Fig. 6. ***Examples of optical platforms for plasmonic biosensors. (a) Spectroscopic system based on intensity measurements and RGB filter. Adapted with permission from [1]. Copyright 2015 American Chemical Society. (b) Phase imaging system. Adapted with permission from [3]. Copyright 2012 American Chemical Society.***

1) Wavelength Interrogation: Measurement of changes in the resonant wavelength (wavelength interrogation) is the most common interrogation method used in affinity biosensors based on plasmonic nanostructures. From an instrumental point of view, wavelength interrogation-based optical platforms typically employ a polychromatic light source [e.g., halogen lamp or superluminescent diode (SLED)] that covers the spectral range in which a plasmonic feature is to be observed. The spectrum of light coupled to an SP is usually acquired by means of a CCD-, complementary metal–oxide–semiconductor (CMOS)-, or PDA-based spectrometer, and the spectral position of the plasmonic feature is tracked using appropriate feature-tracking algorithms. Sensors that exhibit multiple resonances can be handled in a slightly different manner, where the integration of absolute intensity changes over a chosen wavelength range [216]–[218], or similarly, over a range of polarization angles [219], it is used to generate a sensor output.

The properties of spectrometers used in wavelength interrogation-based optical systems influence not only the performance of the sensor, but also its degree of miniaturization, as they require a certain path length to properly disperse light to a position-sensitive detector. The miniaturization of spectroscopic optical systems for plasmonic biosensors has thus recently received a great deal of attention.

Cappi *et al.* proposed a simplification of spectroscopic measurements by retrieval of the spectral feature position from intensity measurements performed by either three spectrally separated diodes [192] or the white light LED source and the CMOS camera equipped with an RGB filter [1] chosen to sample the resonance feature (along with a fast iterative curve-fitting algorithm). Using this approach, they developed a portable sensing device [Fig. 6(a)] and its functionality has been proven in detection of small molecules of tobramycin in blood serum.

Another interesting approach for simplification is to use the dispersive properties of plasmonic nanostructures (that exhibit periodicity) for both a platform for the excitation of surface plasmon modes as well as a dispersive element for a spectrometer. Leong and Guo [220], [221] proposed several plasmonic nanostructures with two different periods, one responsible for the excitation of plasmons and the second acting as a diffraction grating. After integration to a CCD camera, their sensor attained a refractive index sensitivity of around 300 nm/RIU with a resonant wavelength resolution of 0.7 nm.

Another important trend in the development of optical systems for plasmonic biosensors is aimed to increase their throughput, typically achieved with the use of intensity modulation and imaging optical platforms. Ruemmele *et al.* utilized a combination of this approach with an independent spectral analysis of light from multiple sensing regions [222], where plasmonic imaging and spectroscopy were combined in a single optical platform employing a white light source, a liquid crystal tunable filter, and a CCD camera. This system allowed for the simultaneous measurement of intensity and spectra from nine different areas of an array of plasmonic nanodisks. Similar approaches based on hyperspectral imaging and a thin-film-tunable bandpass filter [223] or imaging Fourier transformed spectrometry [224], [225] have also been reported. The main limitation of these approaches is the relatively long time required to collect the full spectrum from either the entire area (on the order of minutes for tunable filters) or from individual NPs (on the order of seconds for imaging Fourier transformed spectrometry).

The problem of lower temporal resolution can be overcome by the integration of a passive dispersive element with the imaging optics. This approach has been recently implemented using a transmission grating placed between the plasmonic nanostructure and microscope objective and used for experiments on individual NPs [226]. For optimal conditions, this approach allowed for the simultaneous acquisition of spectra from 50 individual NPs with a resonant wavelength resolution of 3.8 nm. An improvement of this approach was recently proposed by Liu *et al.* in which

calibration of spectral images (using the cutoff edge of a bandpass filter) allowed for disregarding the zeroth-order images and thus increased the number of collected spectral streaks by up to 500 NPs per frame [227].

2) Intensity Interrogation: The development of plasmonic sensors based on intensity interrogation has been pursued by numerous research groups [228], [229]. These configurations use quasi-monochromatic light sources to excite plasmonic modes, typically in the form of either a laser [15] or an SLED with a narrow emission line. These light sources exhibit better stability and higher intensity than broadband sources combined with narrowband filters, which translate to superior signal-to-noise figures. Changes in the intensity of light coupled to a plasmonic mode are typically measured by means of either a 1-D photodiode array (PDA) or a 2-D detector, such as a CCD or CMOS cameras. In comparison with the wavelength interrogation method, intensity interrogation enables simplification of the optical system (as there is no need for a spectrometer) and more importantly, provides much higher throughput, as imaging of the entire sensing area (potentially comprised of individual sensing spots) can proceed with both high temporal and spatial resolution. Cetin *et al.* recently presented an imaging sensor platform utilizing a battery-powered LED, a CMOS detector, and a plasmonic microarray chip in the form of nanoapertures arranged in six sensing areas [14]. Although this approach resulted in a lightweight, compact platform with multiplexing capability, the resulting refractive index resolution was rather poor (4×10^{-3} RIU). In another approach, Lindquist *et al.* used plasmonic Bragg mirrors surrounding sensing areas (consisting of nanohole arrays) to suppress interference between individual biosensing areas, thus providing the means to increase the density of detection areas on a sensing structure [230]. By using this approach, they demonstrated as many as 600 submicrometer-size sensing areas on a chip, corresponding to a packing density of more than 10^7 per cm^2. High-performance optical systems based on microscope setups have been demonstrated to enable multiplexed sensing on both individual nanoparticles [199] or nanoholes [231]; the latter case demonstrated the simultaneous monitoring of 10 000 nanoholes.

3) Phase Interrogation: In recent years, optical configurations of plasmonic sensors that are based on the interrogation of phase have received a great deal of attention, where various approaches to such interrogation have been developed, most of them retrieving phase information from intensity measurements [232]. The most commonly used approach is based on polarimetry, in which phase information is extracted from the interference of *s*- and *p*-polarized light by means of a polarizer. Their relative phase difference is typically determined from a series of intensity measurements either via angular modulation introduced by a rotating analyzer [233] or via phase modulation introduced by a liquid crystal variable wave plate (LCVWP) and a fixed output analyzer [234]. This is essentially the same principle used in ellipsometry—a well-established method for the characterization of thin films—which makes it possible for phase interrogation-based plasmonic sensors to take advantage of commercially available systems [195]. Ellipsometric experiments using the ATR configuration and an array partially embedded, randomly distributed gold NPs demonstrated a refractive index resolution estimated to be on the order of 10^{-7} RIU [81] or better [83], assuming the accuracy of phase measurements to be 10^{-3}degrees.

Another polarimetric approach is based on analyzing the spatial distribution of the polarization state of a lightwave coupled to a plasmonic mode. Svedendahl *et al.* advanced previous research on SPR phase imaging [235] and presented an LSP-based sensor for phase-sensitive measurements exploiting the ATR configuration [Fig. 6(b)] and a wedge depolarizer (made of two birefringent wedge prisms) that alters the polarization state of light across the illuminated area of a sensor covered with gold NPs [3]. The phase difference between the *p*- and *s*-polarized light results in an interference pattern that varies in response with changes in the refractive index at the sensor surface. This approach was demonstrated to offer an order of magnitude improvement in sensitivity when compared to spectroscopic measurements [3]. Another approach, sometimes referred to as the polarization contrast approach [236], adjusts the phase difference between *s*- and *p*-polarizations to maximize the contrast (and thus the SNR) of the collected image. Piliarik *et al.* used this approach in the ATR configuration, in which an array of gold nanorods was attached to an ATR prism placed between two crossed polarizers and a wave plate (allowing for adjustment of the phase difference) [177]. This system, when compared to the spectroscopy of LSPs, allowed for precision of measurements in the order of 10^{-4} nm.

Table 2 provides an overview of the resolution obtained by systems across all four arrangements. It should be noted, however, that direct comparison of two systems can lead to erroneous conclusions, as the RIU depends on the type (and thus the sensitivity) of a nanostructure, instrumental arrangement, and interrogation scheme.

Systems based on arrays of nanoholes have recently drawn considerable attention, as their performance has approached that of previous SPR systems, albeit achievable in a colinear arrangement. Furthermore, for high-quality elliptical nanohole array introduced into microscope-based instrument, the refractive index resolution has been demonstrated to exceed that of conventional systems based on continuous gold films [29].

Table 2 Examples of Optical Systems With Different Interrogation Schemes and Instrumental Arrangement

Nanostructure	Optical arrangement	Interrogation	Refractive index resolution [RIU]	Ref.
Spherical Au NPs	co-linear - transmission	Wavelength	1×10^{-4}	[5]
Array of Au nanodiscs	co-linear - transmission	Wavelength	1.5×10^{-4}	[13]
Array of Au nanoholes	co-linear - transmission	Intensity	4×10^{-3}, 6.4×10^{-6}	[14, 15]
Array of Au nanoholes	co-linear - transmission	Wavelength	2×10^{-5}	[19]
Array of Au nanoholes	optical microscopy	Wavelength	7.7×10^{-6}, 3.1×10^{-6}	[20, 21]
Array of Au nanoholes	optical microscopy	Intensity	9.4×10^{-8}	[29]
Spherical Au NPs	D-type optical fiber	Intensity	4.1×10^{-4},4.1×10^{-7}	[30, 31]
Spherical Au NPs	U-bent optical fiber	Wavelength or intensity	3.8×10^{-5}	[35]
Spherical Au NPs	U-type optical fiber	Intensity	1.8×10^{-3}, 1.1×10^{-3}	[31, 41]
Spherical Au NPs	optical fiber	Intensity	5.2×10^{-7}	[69]
Au nanorods	optical fiber	Intensity	8.7×10^{-6}	[73]
Array of Aunanorods	ATR	Phase	1.8×10^{-6}	[75]
Spherical Au NPs	ATR	Phase	5.2×10^{-7}	[81]
Array of Au nanospheres	ATR	Phase	$< 10^{-7}$	[83]

In addition to the simplification of the measurement setup, optical fiber-based sensors are simpler in fabrication with respect to their SPR counterparts; however, they are typically based on randomly distributed NPs (limited by fabrication difficulties of more sophisticated structures on the lateral or front fiber surface), which limits the sensitivity of such platforms. The sensitivity of these sensors is dependent both on the applied nanostructure as well as the geometry of the fiber, thus bulk sensitivity is the most common way to compare corresponding systems; however, such comparison does not provide details about capabilities of such system for high-resolution measurements. A simple configuration consisting of a nanoparticle-based U-bent fiber, LED, and fiber-coupled spectrometer [35] was recently shown to exhibit better performance when compared to a colinear transmission-based system [13] of comparable configuration. Moreover, using a noise discrimination scheme (in the form of feedback module), a system consisting of a modulated LED source, a photodiode, a lock-in amplifier, and a straight optical-fiber-based sensor [69] was demonstrated to have a resolution on the same order of magnitude as that of high-resolution prism-based SPR systems [236].

When compared to simple colinear systems, phase-sensitive systems exhibit superior performance; however, in order to take advantage of this approach, a setup needs to be both optimized for resonance conditions and, furthermore, have low levels of instrumental noise; only minor or moderate performance improvements will be realized otherwise.

V. MICROFLUIDIC SYSTEMS

Both the high sensitivity and narrow spectral feature of a plasmonic nanostructure and a low noise readout system are not a sufficient condition to achieve a high-performance sensor. From a practical point of view, a sensor should also have both a fast response (i.e., time-to-result) and a low sample consumption, both of which are expected in point-of-care environments, where the ability to work with limited sample amounts to achieve a rapid, unambiguous diagnose is of high importance. These factors can be controlled by a properly designed microfluidic system, which apart from optimizing sample manipulation in order to improve both temporal response and throughput (e.g., when arranged in multichannel systems), also allows for miniaturization and ease of use. In the last few years, a large amount of work has been directed toward the use of microfluidic systems to improve both the efficiency of analyte delivery (to nanoscopic sensing areas) and the sensor throughput (in multianalyte detection systems). In this section, we present a short overview of recent achievements in this field.

In case of sufficiently low concentration of analyte in the sample, the operation of the sensor in an equilibrium state (where rates of analyte adsorption and desorption are equal) is impractical due to the long times required to reach such state. In this case, an appropriate system for the efficient delivery of analyte to active regions of the sensor surface is necessary.

Typically, a single channel microfluidic chip is used for testing the sensing properties of a given plasmonic structure; however, in order to increase throughput (i.e., in a multianalyte sample), there arises a need for a multichannel microfluidic chip, allowing for precise delivery of liquid samples to multiple detection spots. During the last few years there has been a large effort directed toward the development of multichannel integrated microfluidic chips for sensors based on plasmonic nanostructures; in the current literature such systems can be found to have up to several tens of independent channels [9], [20], [237], [238]. Malic *et al.* [10] presented a thermoplastic microfluidic chip consisting of array of 64 microchambers integrated with plasmonic nanostructures in the form of gold gratings with a nanoslit at the apex of grating structure [Fig. 7(a)]. They are arranged in an 8x8 orthogonal fluidic channel network, where individual delivery of fluids to each chamber is assured by means of an array of pneumatic microvalves. Sensing spots are probed sequentially through alignment to the sensing optics by means of optical XYZ stage. Another multianalyte detection format was recently presented by Chen *et al.* [113], who presented a multilayer system consisting of eight parallel microfluidic channels running across 60 parallel antibody-functionalized AuNR stripes, thus allowing for 480 sensing spots.

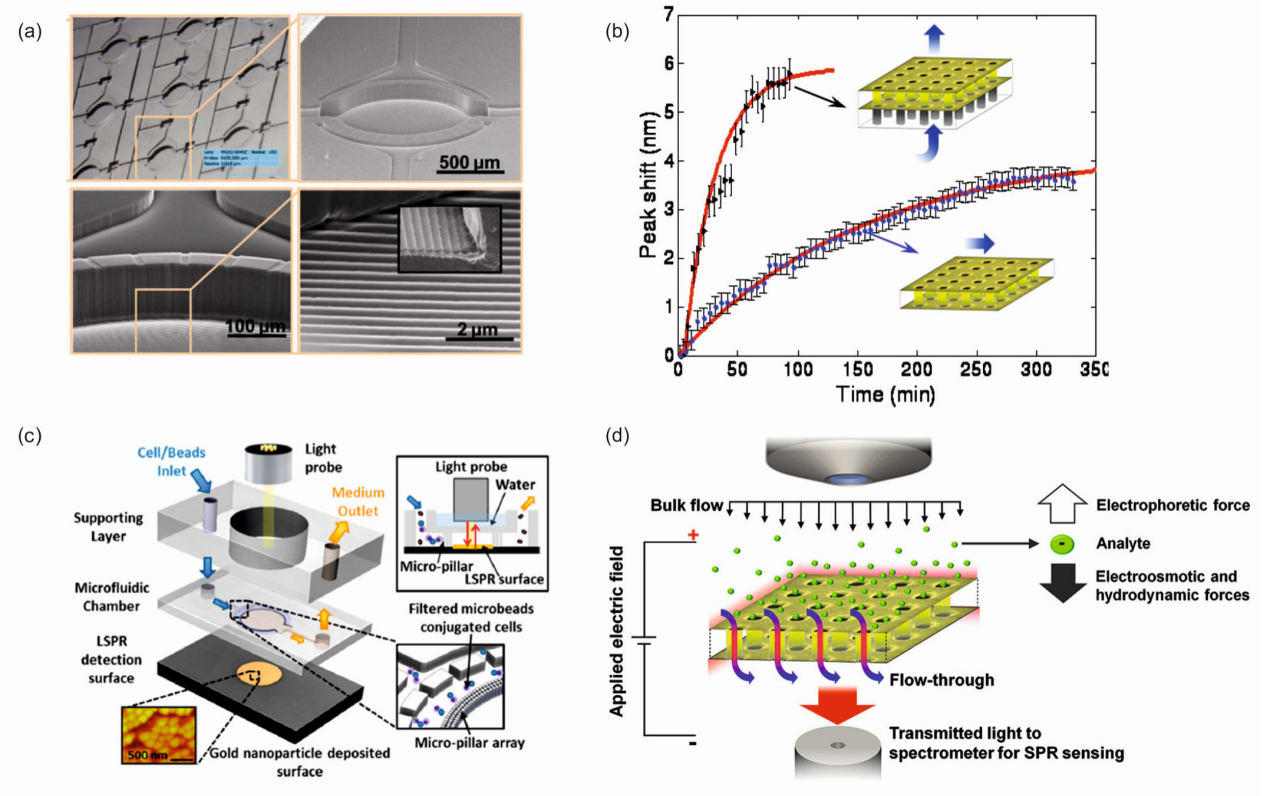

Fig. 7. ***Microfluidic systems. (a) Thermoplastic microfluidic chip integrated with plasmonic nanostructure. Adapted from [10] with permission from the Royal Society of Chemistry. (b) Comparison of response time of sensors based on flow-through and flow-over format. Adapted with permission from [18]. Copyright 2009 American Chemical Society. (c) Integrated system for selective delivery of molecules to sensing area. Adapted with permission from [2]. Copyright 2014 American Chemical Society. (d) System for enhancement of concentrations of target molecules by means of external electric field combined with flow-through format. Adapted with permission from [25]. Copyright 2012 American Chemical Society.***

Similar to their continuous gold film counterparts, the most common arrangement for microfluidic systems is such that a microchannel is sealed directly to the sensing surface, where liquid with target analyte flows over the active sensing regions. As with all affinity biosensors, the tendency of such a system to be either diffusion or interaction limited is determined by a complex interplay between the convection, diffusion, and capture of analyte by immobilized receptors [239]. For interaction-limited systems, changes to the microchannel design (or the sample flow rate) will have no effect on the rate of analyte capture. Conversely, the performance of diffusion-limited sensors can be improved by variety of simple methods, including a reduction of channel dimensions and/or an increase in the flow rate [239], [240]. Nonetheless, in the case of nanostructured sensors working in the flow-over regime, it is hard to achieve a balance between a reasonable time of operation and a low rate of sample consumption; for diffusion-limited sensors, this is not optimal approach, especially when the top surface of a given nanostructure has low sensitivity (e.g., the top surface of a nanohole array). Recently, Ferreira *et al.* [181] have shown that inner walls of nanoholes in an EOT-based sensor give the main input to its response. When fabricated in self-standing membrane, these pores can act as fluidic channels, whereby flowing analyte through the membrane (rather than over) generates an enhancement of the sensor response, primarily due to the increased rate of analyte transport to the active areas of each nanohole. Additional studies on this flow-through approach have showed up to an order of magnitude improvement the sensor response when compared to a flow-over format [Fig. 7(b)] [18], [241]–[243]. Although sensors based on the flow-through approach hold great promise, there are several drawbacks that limit its applicability. Because the premise of such systems is founded on efficient mass transport to the active sensor areas, it will hold greater advantages in diffusion-limited systems (e.g., relatively large analytes having low diffusivity). Conversely, the rate of analyte capture in interaction-limited sensors will be the same across both formats, which exhibit a comparable response [244]. Another limitation comes from the structure itself: nanometer-thick free-standing membranes can be easily deformed by the pressure drop across the membrane, whereby such deformations can affect its optical properties and require the use of lower flow rates [25].

A solution to this problem might be found in another approach utilizing microstructured optical fibers, where inner walls of air capillaries surrounding solid core are covered with AuNPs, whose surface density can be controlled by changing the concentration of NPs (in the solutions used to activate the channels) [245]. In this configuration, fluid flows through the NP activated channels and the optical response is measured in the direction perpendicular to the fiber in transmission mode. The responsivity of such sensors can be controlled by length of the fiber, where the small number of channels can be compensated for by tailoring the interaction length in order to improve collection of target molecules.

In general, the equilibrium level of capture analyte depends on both the concentration of receptors and the kinetics of the affinity interaction, both of which are independent of the flow format. Therefore, despite the improvements in the sensor response time for the flow-through approach, the magnitude of the signal (in an equilibrium state) will be the same as the flow-over format. One direct approach to improve the sensitivity (and limit of detection) of a sensor, regardless of its equilibrium state, is to increase the analyte concentration in the region close to its active area. Escobedo *et al.* [25] proposed a system which combines a flow-through approach and direct current (dc) electric field [Fig 7(d)] to concentrate target molecules in the vicinity of each nanohole (via electric field gradient focusing effects). This approach allowed for an order of magnitude improvement in the sensor response time and, furthermore, a fivefold increase in the peak shift; the expected limit of detection of this approach was about 10 pM for BSA: a two order of magnitude improvement in comparison to nanohole arrays working in the flow-over regime. In a similar approach, Barik *et al.* [246] utilized alternating current (ac) electric field-induced dielectrophoretic (DEP) forces (developed due to a large field gradient at the nanoholes) to actively transport analyte to the metal membrane. This technique combined with the flow-over format allowed for the limit of detection of 1 pM for BSA, where a medium of low conductivity was used to facilitate the effects of DEP. Considering the detection in a complex medium (e.g., blood), the screening effect may reduce the DEP force; moreover, the use of alternating current can increase heat generation and the dissolution of gold, leading to an uncontrollable spectral shift and thus decreasing the precision of measurement. Although these methods clearly hold great promise for use in nanoplasmonic biosensors, there remain a number of constraints that may limit their applicability in more realistic applications.

Another approach lies in the use of microfluidic methods to simplify the protocols related to both sample preparation and detection, both of which are important in point-of-care applications. A recent example of such an approach was shown by Oh *et al.* [2], who presented an integrated system providing the selective extraction of the target analyte from blood and its smart delivery to the sensing area [Fig. 7(c)]. Their microfluidic system consisted of nanopillars set in a circular structure, serving as a filter/trap for polystyrene beads functionalized with immune cells that release cytokines to be detected in the inner region of the structure. The trapping of the beads near the sensing area allows for increase of concentration of target molecules, and thus signal amplification, reduction of the detection time, and a sample volume.

VI. FUNCTIONALIZATION

As research in plasmonics continues to generate nanostructures with potential for optical biosensing, there is a growing demand for methods enabling the functionalization of these nanostructures with biomolecular recognition elements. These biomolecular recognition elements (sometimes referred to as receptors) recognize and capture a targeted molecule (analyte) onto the surface of plasmonic biosensor: a prerequisite for analyte detection by an SP. The immobilization of receptors onto the surface of a plasmonic structure is thus of utmost importance for proper functioning of a plasmonic biosensor and has direct impact on its performance characteristics (sensitivity, specificity, limit of detection). An ideal functionalization method is expected to create a functional coating that: 1) provides a desired concentration of receptors; 2) preserves the biological activity of receptors; and 3) suppresses the nonspecific adsorption of nontarget molecules to the active area of the sensor.

In comparison with the functionalization of continuous metal films used with conventional SPR biosensors, the functionalization of plasmonic nanostructures is much more challenging, as (unlike their flat predecessors) they often comprise multiple materials (e.g., glass and gold) and exhibit surface curvatures (e.g., edges, tips). Moreover, in biosensors based on plasmonic nanostructures, it is preferred that the receptors are not attached to the entire metal surface, but rather to the active areas—hot spots—where the EM field is strongly enhanced. This is achieved through special functionalization methods that enable immobilization of receptors with a spatial resolution.

In this section, we review the main methods used for the functionalization of plasmonic nanostructures, including both the methods that immobilize receptors across entire metal surface and the methods for spatially resolved immobilization of receptors.

A. Functionalization Methods

In order to enable the use of plasmonic biosensors in a broad range of bioanalytical applications, numerous types of receptors (e.g., antibodies, enzymes, peptides, nucleic acids, or aptamers) have been immobilized on plasmonic nanostructures using a variety of functional surface chemistries (based on chemisorption, covalent attachment, affinity-based interactions). Many of the chemistries used

for plasmonic nanostructures have been adapted from those previously used for the functionalization of continuous metal films used with SPR biosensors (for reviews, see [34] and [247]). In this section, we focus on general functionalization strategies that have been successfully utilized with plasmonic nanostructures which typically functionalize the entire metal surface.

The passive adsorption of receptors to the metal surface represents the most simple and straightforward functionalization method; however, it may result in a reduction/loss of biological activity, unfavorable orientation or uncontrollable release of receptors, or high nonspecific adsorption to the functionalized surface [248]. Some of these issues can be alleviated using methods based on chemisorption [249], which take advantage of the strong coordination of sulfur (functional thiol groups on a receptor) and noble metals (typically gold, which is used in majority of plasmonic biosensors). Chemisorption-based methods have been commonly used for the immobilization of thiolated oligonucleotides (ONs) [77], [125] or aptamers [102], [250], [251]. Aptamers are RNA or DNA nucleotide sequences (typically 15–60 base pairs in length) that are selected by an *in vitro* combinatorial process to specifically bind to a target analyte. The immobilization of both ONs and aptamers is typically carried out in a mixture of thiolated oligo-ethylenglycols (EGs), which reduce the density of the receptors and improve the resistance of the coating to the nonspecific adsorption [252], [253]. A similar approach has been used to immobilize thiol-terminated dendrimers or dendrons: repetitively branched molecules, typically symmetric around the core, often adopting a spherical 3-D morphology [115], [254]. Chemisorption has been also employed for the immobilization of antibody single-chain variable fragments (scFvs) [91], [255]. The scFvs contain cysteine residues that enable binding to the metal surface and, at the same time, orient recognition sites toward the sample for target binding [256], [257]. Alternatively, receptors conjugated to gold-binding polypeptide (GBP) can be directly bound to a gold surface via the high-affinity binding between the GBP and gold surface (GBPs are rich in serine and threonine, which coordinate with the gold surface via their polar groups [258]), with binding sites on the receptors accessible for the target [98], [259].

The most widely used functionalization methods are those employing a linker layer. When immobilized to a nanostructure, these linker layers provide a stable surface that can lessen nonspecific adsorption as well as introduce reactive groups for specific and controlled immobilization of a receptor (via covalent coupling or affinity-based interactions). It should be noted that due to the limited decay length of SPs, functionalizations allowing for the binding of analyte molecules close to the metal surface are preferred [255], [260]. Most linker-layer functionalization methods are currently based on the well-established technology of self-assembled monolayers (SAMs) of alkylthiolates. Although there is a variety of alkylthiols with different functional groups, the most commonly used are those containing carboxylic functional groups: when activated, these groups can be used for the covalent attachment of a receptor (via receptor amine groups) [68], [88], [261]. Typically, this process proceeds in a stepwise fashion (formation of SAM, immobilization of receptors); however, some receptors (proteins) have been conjugated to the SAM-forming molecules beforehand for direct immobilization without additional steps [262], [263]. Used to a lesser extent, other functionalization methods include the covalent attachment of amine-terminated receptors to carboxy-terminated amorphous silicon–carbon alloy films [264], [265] or zwitterionic copolymers [266], [267]. Amine coupling chemistry can also proceed in an inverse arrangement, where a layer of cystamine (bearing thiol- and amine-group) was used to covalently attach carboxy-terminated receptors, including antibodies [149], [207] or phytochelatins [148]. Amine-terminated surfaces (created by plasma polymerization-assisted surface modification) have been used to immobilize amine-terminated receptors via glutaraldehyde crosslinker [268].

Affinity interactions (e.g., host–guest or avidin–biotin interactions) present an interesting alternative to the covalent attachment of receptors to a linker layer. Thiolated calixarene molecules have been demonstrated to efficiently immobilize antibodies (with favorable orientation) via host–guest interaction [269]. In another work, a gold surface was modified with a poly[3-(pyrrolyl)carboxylic acid] film, whereby the carboxylic functional groups were coordinated with Cu^{2+} ligand for the immobilization of histidine-tagged peptides [270].

The functionalization of metal nanostructures can be also performed by using photoactivable reagents. Photoinduced surface functionalization has been demonstrated by Gschneidtrier *et al.*, who coated a metal surface with thiolated photoactive molecules, to which a biotinylated linker was coupled upon exposure to UV light. Subsequently, the biotin-modified surface was used to attach avidin-conjugated molecules [271].

B. Spatially Resolved Functionalization Methods

In order to take advantage of the local confinement of the EM field (hot spots) on plasmonic nanostructures, there are currently several research efforts toward functionalization methods enabling the localized immobilization of receptors with a spatial resolution of the size of each hot spot. Taking into account the typical feature size of plasmonic nanostructures (<100 nm), the spatially selective delivery and immobilization of receptors onto the surface of a nanostructure is clearly a challenging task. To date a few approaches have been proposed to address this challenge, including methods based on material selective chemistry, contact printing, place-exchange chemistry, molecular imprinting, and light-assisted immobilization.

Material-selective functionalization methods have been mainly exploited for the functionalization of arrays of nanoholes, where receptors are preferred to be anchored to the inner walls of each nanohole (regions with the highest sensitivity) and the surface outside the nanoholes should be functionalized to prevent analyte binding. This task was tackled by Fereirra *et al.* [181], who fabricated nanoholes in SiO_x/Au film on a glass substrate; a material-specific cysteamine/biotin-based surface chemistry was used to promote specific binding of streptavidin to the Au regions only.

Similar functionalization for in-hole sensing was presented by the research group of Höök, who fabricated nanoholes in a TiO_2/Au/TiO_2 film on a glass substrate [183] and a SiN/Au film on a silicon wafer [242]. They used a material-specific surface chemistry combing thiolPEG/thiolPEGbiotin mixture (efficiently adsorbing on gold but not on TiO_2 or SiN) and PEG grafted to poly-L-lysine (adsorbing on TiO_2 or SiN but not on the functionalized gold surface). They demonstrated highly selective binding to biotin immobilized on the inner walls (by a factor of 20 when compared to experiments where avidin was allowed to bind across the entire sensor surface) [183]. Later, Feuz *et al.* used the material-selective surface chemistry for controlled immobilization of receptors in the gap between pairs of nanodisks [182]. This functionalization approach increased the sensor response (measured per bound molecule) by a factor of four compared to binding to single disks (bulk sensitivity and binding area were taken into account).

A functionalization method based on contact printing was proposed by Lin *et al.* in order to immobilize receptors inside nanopits [180]. In the first step, the flat regions around the pits were passivated with a layer of EG_3-terminated disulfides created by the contact printing. The nanostructure was then immersed in a maleimide solution allowing for directed immobilization of the thiol-terminated disaccharide receptors to the maleimide groups inside the pits. The functionalization approach was evaluated in a model biosensing experiment; the authors demonstrated that this functional surface provided two times higher sensor response than a reference surface produced by uniformly coating the nanostructure with a maleimide/EG_3-disulfide mixture.

Another interesting approach to the spatial functionalization of nanostructures is based on thiol exchange chemistry. Beeram and Zamborini used this approach to immobilize anti-IgG antibodies on the edges of Au nanoplates [260], [272]. In the first step, they covered an Au surface with a SAM of thiolates having hydroxylic terminal groups, after which an induced exchange of thiol molecules was accomplished by adding a solution containing thiols having a carboxylic group. Due to the reduced steric hindrance at the high-curvature areas, thiol molecules located on the edges of the nanoplates are more readily exchanged with thiols in solution (with respect to those located on the flat regions) [273]. The enhanced concentration of carboxylic groups (and subsequently attached antibodies) at the edges of nanoplates was confirmed in model sensing experiments; the sensor response to the binding of IgG (to immobilized anti-IgG) was found to be four times higher than that obtained using nanoplates covered only with a carboxy-terminated SAM.

Abbas *et al.* demonstrated the spatial functionalization of gold nanorods using molecularly imprinted polymer (MIP) [274]. This method involved adsorption of a thiol-terminated linker molecule and subsequent attachment of protein template to the tips of Au nanorods, followed by siloxane polymerization and MIP formation. The adsorption of the linker molecule occurred mainly at the nanorod tips, as they are known to be less covered by CTAB compared to the side walls of the nanorod [275]. The final release of the protein template created a polymeric recognition cavity that acts as an artificial receptor for target analyte.

Recently, a light-assisted method for the controlled immobilization of proteins into the gaps of plasmonic dimers was proposed by Galloway *et al.* [276]. In this method, a droplet containing the protein was allowed to evaporate over the nanostructures. Upon illumination, disulfide bridges in the protein (present in the dimer gap) were disrupted by three-photon absorption of UV photons by the nearby aromatic amino acids, whereby the resulting thiol groups were used for the immobilization of proteins. Using this method, molecules of BSA were immobilized in the gaps of Au dimers, biotinylated, and used to attach streptavidin-coated AuNPs.

VII. APPLICATIONS

Biosensors based on plasmonic nanostructures have been applied toward various problems in both bioanalytics and molecular biology. Among others, bioanalytical applications have included the detection and quantification of chemical and biological analytes; these are reviewed in Section VII-A. Applications of plasmonic biosensors in molecular biology have been mainly concerned with the investigation of biomolecules and their interactions; a review of these applications is provided in Section VII-B.

A. Bioanalytical Applications

Biosensors based on plasmonic nanostructures have been applied to detection of chemical and biological analytes related to medical diagnostics, environmental monitoring, food safety, and security. This section describes the most commonly used detection methodologies (detection formats) and reviews the state of the art in applications of biosensors based on plasmonic nanostructures in these areas. Examples of important bioanalytical applications are collected in Table 3.

Table 3 Selected Examples of Applications of Plasmonic Biosensors for Detection of Chemical and Biological Species. The Experiments Were Performed in Air and Performance Characteristics Were Determined in Buffer Unless Otherwise Stated

		Measurement mode (Detection time)	Performance	Nanostructure	Ref.
Medical diagnostics					
AFP PSA	Liver cancer Prostate cancer	Continuous (15 min, under flow)	1 ng/ml (50% serum) 0.5 ng/ml (50% serum)	Au nanorods	[9]
PSA	Prostate cancer	Continuous (2 hrs, static sol.)	1 pM	Au nanodiscs	[16]
PSA	Prostate cancer	Continuous (5 min, static sol.)	1 pg/ml	sAuNPs	[22]
PSA-ACT complex	Prostate cancer	End-point (1 hr)	111 aM	Individual Au nanorods	[24]
AFP	Liver cancer	End-point	0.85 ng/ml (buffer) 3.3 ng/ml (100% serum)	sAuNPs	[32]
AFP	Liver cancer	End-point (30 min)	24 ng/ml	Au nanomushrooms	[47]
HE4	Ovarian cancer	End-point (40 min)	4 pM	AgNPs	[68]
SCCa	Cervical cancer	End-point (30 min)	0.125 pM	AgNPs	[71]
SNP in *K-ras* gene	Colon cancer	End-point (2 hrs)	10 nM	Au nanorods	[74]
MutS protein Telomerase	Mutation-induced cancer Cancer cells	End-point (1 hr)	N/A 10 HeLa cells	Individual sAuNPs	[77]
ctDNA	Mutation-induced cancer	End-point (30 min)	50 fM (50% serum)	Individual sAuNPs	[78]
5-methylcytosine MBD2 protein	Epigenetic changes	End-point (2 hrs)	1 molecule 125 fM MBD2	Individual Au nanostars	[82]
L2 zinc domain of p53	Mutation-induced cancer	End-point (2 hrs)	10 nM	Ag nanotriangles	[86]
Intact HIV virus	AIDS	End-point (1 hr)	98 copies/ml (100% blood)	sAuNPs	[88]
HIV-1 particles	AIDS	End-point	200 fg/ml	AuNPs	[91]
HBV surface antigen HBV antibody	Hepatitis B	End-point (1 hr)	100 pg/ml 1 pg/ml	Au-capped NPs (core-shell AuNPs)	[98]
VSV; Ebola; Vaccinia viruses	Enveloped RNA/DNA viruses	End-point (1.5 hr) Flow-through system	10^6 pfu/ml	Au nanoholes	[101]
L. acidophilus; S. typhimurium; P. aeruginosa	Pathogenic bacteria	End-point (1 hr)	10^4 cfu/ml	Au-capped NPs (core-shell AuNPs)	[102]
V. vulnificus Salmonella spp.; S. aureus; Enteroc. Faecalis; N. gonorrhoea; S. epidermidis; K. oxytoca	Pathogenic bacteria	End-point	N/A	Cu-capped NPs (core-shell CuNPs)	[106]
EAP	Bacterial pathogen	Continuous (2 hrs, static sol.)	8 pM	Au nanodiscs	[16]
IFN- γ	Inflammation	Continuous (5 min, static sol.)	2 pg/ml	sAuNPs	[22]
TNF-α	Inflammation	Continuous (under flow) On-chip cell trapping	from 1000 cells	sAuNPs	[2]
TNF-α; IFN- γ; IL-2; IL-4; IL-6; IL-10	Inflammation	Continuous multianalyte detection (under flow)	11 pg/ml; 6 pg/ml; 21 pg/ml; 5 pg/ml; 11 pg/ml; 11 pg/ml	Au nanorods	[113]
Anti-AXO IgG	Immune response	Continuous (30 min, under flow)	0.6 ng/ml	Au nanodiscs	[115]
Allergen specific IgG	Immune response	Continuous (15 min, under flow)	2 nM	Array of AuNPs	[117]
HSA	Microalbumineria	End-point (30 min)	1 ng/ml	AgNPs	[122]
BIGH3 gene	Corneal dystrophy	End-point (6 hrs)	1 pM	Au-capped NPs	[124]
DNA targets	Lactose intolerance	End-point (3 hrs)	N/A	Individual Au nanotriangles	[125]
Glucose	Metabolism	End-point (30 min)	25 μM (buffer) 50 μM (filtered bovine plasma)	Au nanoprisms	[129]
Food safety					
Salbutamol	Drug residue	End-point (1 hr at)	10 ng/ml	Ag nanotriangles	[134]
Salbutamol	Drug residue	End-point (1 hr at)	20 ng/ml	Hollow AuNPs	[135]
Pentagalloyl glucose	Polyphenol	End-point (3 min, under flow)	0.5 μM	Au nanodiscs	[136]
Bovine somatotropin	Drug residue	End-point (40 min)	5 ng/ml	Au nanoislands	[137]
Ricin; Shiga toxin; Cholera toxin	Toxins	Continuous (20 min, under flow)	30 ng/ml; 10 ng/ml; 20 ng/ml	sAuNPs	[139]
Ochratoxin	Mycotoxin	End-point	1 nM	Au nanorods	[141]
Environmental monitoring					
Pd^{2+}	Heavy metal ion residues	End-point (5 min)	5 nM	Au nanoislands	[143]
Cd^{2+}	Heavy metal ion residues	End-point (10 min)	0.1ppb	sAuNPs	[148]
Other applications					
cGMP	Intracellular messenger	End-point (2 hr)	0.1 nM	sAuNPs	[149]
Ca^{2+}	Intracellular messenger	Continuous (30 min, under flow)	23 μM	Ag nanoprisms	[150]
RS-melagatran	Anticoagulant drug	End-point (under flow)	0.9 nM	Au nanorods	[151]
RS-TNA	Drug intermediate	End-point (under flow)	10 nM (*R*); 150 nM (*S*)	Au nanorods	[152]

1) Detection Formats: The sensitivity of biosensors based on plasmonic nanostructures decreases with increasing distance from biosensor surface; therefore, in order for a detection format to be useful, changes in the refractive index must occur in a region close to the nanostructures. It follows that most research is focused on the direct detection of analyte, in which the biosensor responds to the binding of analyte directly to a receptor immobilized on the surface. Although direct detection provides several benefits, primarily in the speed and simplicity of analysis, it may not provide the sensitivity required for many bioanalytical applications of interest and, furthermore, may suffer from interferences (e.g., nonspecific adsorption) from complex samples (e.g., bodily fluids, foods). In order to overcome these limitations, approaches that enhance the sensor response (or the contrast between the specific and nonspecific binding) are often used. The most straightforward enhancement strategy involves the use of a second biorecognition element (e.g., antibody) that binds to previously captured analyte; this approach is sometimes referred to as sandwich detection format. To further enhance the sensor response, the second biorecognition element can be labeled with a tag (e.g., a gold nanoparticle—AuNPs) or an enzyme (e.g., horseradish peroxidase); however, due to the limited decay length of the EM field on typical plasmonic nanostructures, the enhancement generated by large tags (e.g., AuNPs) is usually not as impressive as in the case of conventional SPR biosensors [277].

There have been several examples of the use of enhancement techniques used in nanoplasmonic biosensors. A secondary antibody was employed in a sandwich assay for the detection of human α-thrombin by Guo and Kim, who demonstrated a 2.5-fold enhancement of the sensor response due to the antibody [251]. An AuNP-labeled secondary antibody was used to enhance the sensor response to a model analyte (biotin) by Hall *et al.*, who demonstrated a fourfold enhancement due to the AuNP-labeled antibody [278]. A similar level of enhancement was achieved by Nguyen *et al.*, who exploited AuNPs-labeled antibodies to detect epigenetic methylations in circulating tumor DNA [78]. A tenfold enhancement was obtained by means of both Au nanorods and Au nanostars attached to DNA strands (complementary to the target DNA) when compared to nonlabeled complementary DNA [279]. In the work of Schneider *et al.* [280], a threefold enhancement of the sensor response to the hybridization was achieved when streptavidin-coated AuNPs were applied after the hybridization of biotinylated complementary DNA.

An enzymatic enhancement strategy was used by Lee *et al.* for the detection of interferon-γ [281]. They used biotinylated secondary antibody and a horseradish peroxidase (HRP) conjugated with avidin. The HRP-catalyzed precipitation was found to enable the detection of hundredfold lower concentration of interferon-γ than in the case of detection without the enzymatic reaction.

2) Cancer Biomarkers: Among all the analytes related to medical diagnostics, cancer biomarkers have received the most attention. These applications have included both the detection of cancer biomarkers in circulatory systems as well as the investigation of changes in specific human genes associated with cancer development.

Acimovic *et al.* [9] demonstrated the detection of human alpha-feto-protein (AFP, cancer of liver, testes, and ovaries) and prostate-specific antigen (PSA, prostate cancer) in 50% human serum using a sandwich detection format and an integrated optofluidic device. Specific antibodies were covalently attached to the alkylthiolate SAM on the surface of Au nanorods and 1% human serum was used as a blocking agent. Cancer biomarkers were detected at levels down to 0.5 ng/ml (PSA) and 1 ng/ml (AFP), with a reproducibility exceeding 97%.

Other published works targeting PSA have been performed in buffer rather than in bodily fluids. Direct detection of PSA in buffer was demonstrated by Chen *et al.* [16], who used anti-PSA antibodies covalently attached to Au nanorods functionalized with an alkylthiolate SAM; the LOD was estimated to be 1 pM. Direct detection of PSA (down to 1 pg/ml) in buffer was also demonstrated by Jeong *et al.* [22], who used an optical fiber plasmonic sensor with anti-PSA immobilized (via simple physisorption) to the sAuNPs on the end-face of the fiber, along with BSA as a blocking agent. The complex of PSA with α_1-antichymotrypsin (ACT) was detected by Troung *et al.* [24] using a plasmonic sensor based on the spectroscopy of individual Au nanorods (in an array). In their work, monoclonal antibodies against PSA were covalently attached to an alkylthiolate SAM on the Au nanorodes via amine coupling; PSA–ACT was detected at concentrations as low as 111 aM.

A plasmonic biosensor based on a U-bent optical fiber for the detection of AFP was reported by Liang *et al.* [32]. sAuNPs were attached to the surface of the fiber and functionalized with thiourea, which were then used for the covalent attachment of AFP antibody (using glutaraldehyde as a cross linker). Calibration curves were established both in buffer and spiked undiluted human serum (using BSA as a blocking agent) with LODs of 0.85 ng/ml and 3.3 ng/ml, respectively. In addition, the analysis of clinical serum samples compared well with those obtained using the ELISA method ($R^2 = 0.9873$). Recently, Li *et al.* [47] reported on the use of Au nanomushrooms coated with alkylthiolate SAM and functionalized by the covalent attachment of anti-AFP; AFP was detected in buffer with a LOD of 24 ng/ml. The feasibility of this approach was evaluated in proof-of-concept experiments in which AFP was detected in serum samples collected from the patients suffering from liver cancer. To reduce the nonspecific adsorption from serum samples, surface of the sensor was blocked using either BSA or human serum from heathy donors.

The detection of human epididymis secretory protein 4 (HE4), an ovarian cancer biomarker, was demonstrated by Yuan *et al.* using AgNPs coated with an alkylthiolate SAM to which specific antibodies were covalently attached [68]. The sensor was able to detect HE4 in buffer with a LOD of 4 pM; experiments carried out with serum samples showed a very good correlation ($R^2 = 0.926$) with results obtained by ELISA. Using the same approach, this group also demonstrated the detection of squamous cell carcinoma antigen (SCCa), a cervical cancer biomarker, with a LOD in buffer as low as 0.125 pM [71]; the analysis of serum samples from cancer patients revealed significantly increased levels of SCCa when compared to those of healthy donors.

Dodson *et al.* reported the detection of single nucleotide polymorphisms (SNPs) in codon 12 of the *K-ras* gene, frequently occurring in early stages of colon cancer [74]. In this report, thiolated DNA probes (17mer) were immobilized onto Au nanorods, after which hybridization with fully matched (WT) or 1 b.p. mismatch (MT) complementary strands was performed in buffer. Then, a nuclease was introduced that specifically cleaves imperfectly hybridized duplexes (MT) while maintaining the perfectly hybridized ones (WT) intact. This enzymatic cleavage-based assay was shown to discriminate the presence of SNPs down to 10 nM in the presence of hundredfold concentrations of the WT DNA in buffer [74]; the LOD for the WT DNA was 2 nM.

Ma *et al.* used a biosensor based on individual sAuNPs (and the specific binding of enzymes to their nucleic acid substrates) for the qualitative discrimination of both a mutant gene from a normal gene and a cancer cell from a normal cell [77]. In this work, thiolated DNA substrates (46mer probes) were immobilized onto the surfaces of the AuNPs in a mixture with OEG_3 and used for two proof-of-concept experiments. In the first experiment, a mutant gene was detected both in buffer and in diluted human serum via the specific binding of MutS (a DNA mismatched repair protein that has a close correlation with gene mutation-induced cancer) to a mismatched duplex; prior the MutS binding, the mismatched duplex was created through hybridization of mutant DNA with the immobilized DNA. In the second experiment, human telomerase (overexpressed in cancer cells) was detected (down to 10 HeLa cells) via the binding of telomerase to its substrate and elongation of the substrate due to the presence of dNTPs in diluted extract from the cells.

Circulating tumor dsDNA (ctDNA, 69mer) bearing tumor-specific mutations and epigenetic modifications was detected in 50% blood serum by Nguyen *et al.* [78]. In this work, peptide nucleic acid (PNA) probes were covalently attached to sAuNPs coated with an alkylthiolate SAM and used to capture ctDNA; the LOD for ctDNA (in 50% blood serum) was as low as 200 fM. Furthermore, they used AuNPs functionalized with anti-methyl group antibodies to detect epigenetic methylations in the ctDNA and to further enhance the sensor response to the ctDNA binding; the AuNPs improved the LOD by a factor of four.

An epigenetic study of the p53 promoter was reported by Nguyen *et al.* [82], who used a PNA-functionalized plasmonic biosensor for the detection of two epigenetic biomarkers: methyl-CpG group and methyl-CpG binding domain protein 2 (MBD2). PNA probes were immobilized to Au nanostars functionalized with the p53 promoter (via an alkylthiolate SAM) and hybridized with both the p53 promoter and its modified alternatives. The platform was used for the following experiments: 1) assessment of binding of MBD2 to the methyl-CpG sites, and subsequent analysis of the steric competition between MBD2 and transcription factors; 2) monitoring of the stiffness of methylated p53 promoters by analyzing their structural bending (detected by a plasmon coupling mode between two Au nanostars placed at the opposite ends of respective promoters); and 3) real-time monitoring of epigenetically mediated suppression of transcription. In buffer, the biosensor was able to detect one 5-methylcytosine molecule and the LOD for MBD2 was established to be 125 fM. They also demonstrated that DNA methylation and MBD2 can be detected in lysates extracted from HeLa and HEK cells. The detection of mutations in the p53 gene was also demonstrated by Duan *et al.* [86], who used a plasmonic biosensor based on Ag nanotriangles, functionalized with amine-terminated DNA probes covalently attached to an alkylthiolate SAM. They were able to detect both mismatches in the p53 sequences (LOD 10 nM in buffer) as well as PCR products amplified from the genomic DNA of an ovarian cancer patient; the difference between wild-type and mismatched p53 DNA were shown to be significant.

3) Bacteria and Viruses: The simultaneous detection of three different bacteria (*L. acidophilus, S. typhimurium, and P. aeruginosa*) was shown by Yoo *et al.*, who used core-shell AuNPs coated with bacteria-specific aptamers terminated with thiol groups [102]. The LODs for all three bacterial species were as low as 10^4 cfu/ml (in buffer).

The multiplexed detection of bacterial DNA (*Vibriovulnificus* (119mer), *Salmonella spp.* (138mer), *Staphylococcus aureus* (194mer), *Enterococcus faecalis* (353mer), *Neisseria gonorrhea* (1236mer), *Staphylococcus epidermidis* (202mer) and *Klebsiella oxytoca* (434mer)) was reported by Kim *et al.* [106]. They used a multispot array of core-shell CuNPs functionalized with thiolated DNA probes to monitor the hybridization of target sequences having various lengths. The assay was optimized with seven DNA targets isolated from bacteria strains and amplified by PCR. No cross reactivity was observed and LODs determined in deionized water (hybridization probably enabled due to the residual salts from PCR amplification) were 1 pM for *V. vulnificus*, *Salmonella spp*, *S. aureus*, and *S. epidermidis*, 100 fM for *E. faecalis* and *K. oxytoca*, and 10 fM for *N. gonorrhea*, respectively. The performance of this approach was also assessed in a clinical setting, where seven blind samples isolated from various clinical specimens including blood,

pus, sputum, and urine were tested and the results were compared with those obtained from culture-based assays.

Detection of extracellular adherence protein (EAP) present on the outer surface of the bacterium *Staphylococcus aureus* was demonstrated by Chen *et al.* [16]. In this work, antibodies against EAP were covalently attached to alkylthiolate SAM functionalized Au nanorods; the reported LOD in buffer was estimated to be 8 pM.

The detection of HIV-1 like particles was reported by Lee *et al.*, who used anti-gp120 antibody fragments immobilized to the surface of AuNPs (via chemisorption of thiol groups); the direct detection of HIV-1 like particles (captured via the gp120 proteins on their surface) was demonstrated at concentrations as low as 200 fg/ml [91]. The same capture mechanism was employed by Inci *et al.* [88], who immobilized biotinylated anti-gp120 antibodies to the surfaces of NeutrAvidin-coated sAuNPs and detected intact HIV virus in both commercial virus-free blood spiked with six different HIV subtypes as well as in clinical blood samples. They were able to detect 98 copies of the HIV virus in one ml of whole blood with a reproducibility ranging from 56% to 96%, depending on HIV subtype.

Another example of direct detection of intact viruses was presented by Yanik *et al.* using an Au nanohole array functionalized with specific antibodies (via Protein A/G microspotted on the sensor surface) [101]. Three viruses—vesicular stomatitis virus, pseudotyped Ebola, and vaccinia virus—were detected at clinically relevant concentrations (10^6 PFU/ml), both in buffer and cultivation medium.

A plasmonic biosensor for the detection of hepatitis B virus in buffer was developed by Zheng *et al.* [98]. The authors employed core-shell AuNPs functionalized with GBP fusion protein for the detection of HBV surface antigen (HBsAg) and anti-HBsAg antibody in buffer; the lowest concentrations detected were 100 pg/ml and 1 pg/ml for HBsAg and anti-HBsAg, respectively.

4) Immunity System Response Biomarkers: An integrated optofluidic detection platform for cell-secreted tumor necrosis factor cytokine (TNF-α) in clinical blood samples was reported by Oh *et al.* [2]. In this work, cells were first trapped by an array of nanopillars and subsequently stimulated by an endotoxin solution. This initiated the secretion of cytokines from the cells, which diffused to the detection region of the system where they were captured by the specific antibodies covalently attached to the sAuNPs surface (Fig. 8). This detection approach was tested in buffer and then applied to cells isolated directly from human blood; the platform was capable of detecting TNF-α secreted from as few as 1000 cells.

Chen *et al.* reported an integrated system for the parallel detection of six cytokines (interleukin-2, interleukin-4, interleukin-6, interleukin-10, interferon-γ, and TNF-α) using an array of Au nanorods functionalized with specific antibodies

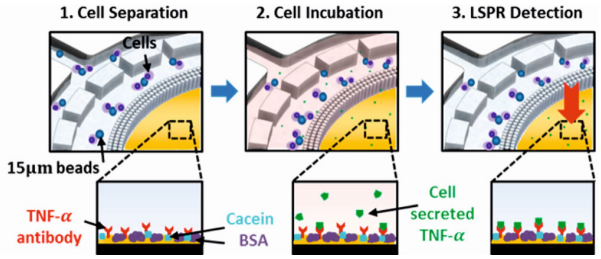

Fig. 8. ***Assay principle of detection of cell-secreted TNF-α. Adapted with permission from [2]. Copyright 2014 ACS Publication.***

(covalently attached to an alkylthiolate SAM), where BSA and casein were used to reduce the nonspecific adsorption [113]. They demonstrated LODs as low as 5-21 pg/ml (in buffer) across all cytokines. The approach was applied to cytokines spiked into heat inactivated and charcoal adsorbed human serum; results correlated well with ELISA ($R^2 = 0.973$). This biosensor was able to monitor the inflammatory responses of infants following cardiopulmonary bypass surgery through tracking the time-course variations of their serum cytokines. A similar LOD (2 pg/ml) for the detection of interferon-γ in buffer was achieved by Jeong *et al.* [22], who used an optical-fiber-based biosensor having sAuNPs functionalized with antibodies against interferon-γ (via simple physisorption) on the end-face of the fiber, with BSA as a blocking agent.

Recently, a plasmonic biosensor for the diagnosis of amoxicillin (AX) allergy was proposed by Soler *et al.* [115]. In order to detect specific IgE generated during an allergy outbreak, the authors functionalized Au nanodiscs with a custom-designed thiolated dendron. To reduce the nonspecific adsorption, 2% commercial serum was used and the SiO_2 part of the sensor was blocked with polylysine-PEG. The LOD for the detection of specific IgE was determined to be 0.6 ng/ml. This assay was used to quantify levels of anti-AX antibodies in patients' serum; results were validated using conventional clinical immunofluorescence assay techniques ($R^2 = 0.999$).

The detection of allergen-specific antibodies in 10% delipidated serum, whole blood, and heparin stabilized blood was reported by Olkhov *et al.* [117]. They used an array of AuNPs functionalized with four different allergens (cat dander, dust mite, peanut allergen, and dog dander) by inkjet printing and the respective anti-allergen IgG antibodies were detected using a sandwich assay with secondary anti-IgG antibodies. The LOD was estimated to be of 2 nM, where fibrinogen coated spots served as a reference.

5) Drug Residues: The detection of salbutamol (Sal) was demonstrated by the group of Di [134], [135]. Sal is being abused as a growth promoter and fattening agent in animals and its residues can cause health problems in humans. In their approach, anti-Sal antibodies were adsorbed onto either Ag nanotriangles [134] or hollow

AuNPs [135], followed with BSA blocking. Sal was detected in buffer with a LOD of 10 ng/ml and 20 ng/ml for the Ag and Au nanostructures, respectively. In proof-of-concept experiments, the analysis of the supernatant from homogenized and centrifuged samples (from animal feed, milk, and pork liver samples) showed a very good recovery for both the Ag and Au nanostructures.

The detection of a recombinant growth hormone, bovine somatotropin (bST), was performed by Ozhikandathil *et al.* [137]. They used a sensor based on Au nanoislands functionalized with specific antibodies (covalently attached via an alkylthiolate SAM). A nonfat milk powder solution was used as a blocking agent, and bST was detected in buffer at concentrations down to 5 ng/ml.

6) Toxins: A portable biosensor system for quantitative detection of toxins utilizing glyco-chips was developed by Nagatsuka *et al.* [139]. Ricin, Shiga toxin, and cholera toxin were detected in buffer via their specific binding to sAuNPs functionalized with synthetic glycosyl ceramides. The selectivity of their assay was verified by experiments with inhibitor or reference proteins. The LODs demonstrated for the detection of toxins in buffer were 30 ng/ml, 10 ng/ml, and 20 ng/ml for ricin, Shiga toxin, and cholera toxin, respectively.

The detection of a mycotoxin, ochratoxin (OTA), was reported by Park *et al.* [141]. Their approach was based on the binding of OTA to Au nanorods functionalized with an OTA aptamer. The binding of OTA induces aptamer folding to form a G-quadruplex structure, which leads to an increase in the density and a decrease in the thickness of the OTA aptamer complex. This approach was demonstrated to enable the detection of OTA in buffer with a LOD as low as 1 nM. In addition, the quantitative determination of OTA in spiked corn samples was shown to have a very good recovery.

7) Heavy Metals: An interesting strategy for the detection of Pd^{2+} was proposed by Gao *et al.* [143], who used Au nanoislands functionalized with a small organic molecule HSPh-bpy-PhSH (Comp1) via a thiol group. This Comp1 molecule exhibits a high affinity to Pd^{2+} via complexation with a square-planar configuration of Pd; the system is reversible as Pd^{2+} can be readily decomplexed using ethanoldiamine. They demonstrated the detection of Pd^{2+} ions in dioxane solution with a LOD of 50 nM.

The detection of Cd^{2+} in buffer was performed by Lin *et al.* [148], who used an optical fiber-based biosensor with sAuNPs functionalized with cystamine and phytochelatins (PCs) that were covalently attached via amine coupling. PCs are heavy metal ion binding peptides, which are capable of chelating Cd^{2+} by thiolate coordination because of a high content of cysteine residues. In experiments performed in buffer, Cd^{2+} ions were detected with LOD of 0.16ppb.

8) Other Analytes: Lai *et al.* reported the detection of human albumin in urine, the abnormal presence of which (microalbumineria) is an independent risk factor of cardiovascular diseases [122]. Using a biosensor based on AgNPs functionalized with antibodies specific to human albumin (covalently attached to an alkylthiolate SAM), albumin was detected both in phosphate buffer and in 0.1% urine samples; the LOD for the detection in buffer was 1 ng/ml.

Yoo *et al.* demonstrated the detection of DNA point mutations in the human transforming growth factor induced (*BIGH3*) gene associated with corneal dystrophy (CD) [124]. Amine terminated DNA probes were covalently attached to dithiodibutiric acid functionalized Au-capped NPs and hybridized with PCR-amplified DNA targets. Three different single point mutations and six different target lengths were studied; the LOD for the detection in buffer was 1 pM.

A plasmonic biosensor for the detection of glucose was proposed by Joshi *et al.* [129], who exploited Au nanoprisms functionalized with a poly(allylamine) polymer (covalently attached to a alkylthiolate SAM). The release of protons from the enzymatic catalysis of glucose (by dissolved glucose oxidase) induced conformational changes of the polymer. In model experiments, this biosensor was able to detect glucose at levels down to 25 μM and 50 μM in buffer and filtered blood plasma, respectively.

An optical platform with integrated microfluidics for the detection of anticoagulant drug melagatran was developed by Guo *et al.* [151]. The detection approach relied on the chiral discrimination of the *RS*-melagatran by using Au nanorods functionalized with human α-thrombin (covalently attached to an alkylthiolate SAM). The detection of *RS*-melagatran was performed in buffer with a LOD of 0.9 nM; results showed that the presence of 10 000-fold excess of the corresponding enantiomer counterpart (*SR*-melagatran) did not interfere with the detection. Proof-of-concept experiments were also performed in human serum. This concept was further expanded for the determination of a racemic mixture of (*R*)- and (*S*)-1,2,3,4-Tetrahydro-1-naphthylamine (TNA), which is a drug intermediate [152]. They used a dual-channel measurement system with a weak chiral receptor (HSA) in one channel and a nonenantioselective receptor (TNA antibody) in the other. Both receptors were immobilized to Au nanorods via amine coupling to a PEG-thiol acid SAM. The LODs in buffer were determined to be 150 nM for (*R*)-TNA and 100 nM for (*S*)-TNA, respectively.

The detection of a low molecular weight polyphenol molecule, pentagalloyl glucose (PGG), via its interaction with amylase (AMY) was reported by Guerreiro *et al.* [136]. Using Au nanodiscs functionalized with AMY (covalently attached to an alkylthiolate SAM via amine coupling chemistry), they were able to detect PGG in buffer down to 0.5 μM. This assay was used for the analysis of 1% wine samples with a good recovery.

A plasmonic biosensor used for the detection of Ca^{2+} was presented by Hall *et al.* [150], who exploited conformational changes of immobilized calcium-sensitive protein calmodulin to quantify calcium ions concentration. A recombinant calmodulin–cutinase construct was immobilized to phosphonate-terminated SAMs on the surface of Ag nanoprisms via a covalent bond between the cutinase and phosphonate groups; a LOD in buffer was demonstrated to be 23 μM.

Huang *et al.* demonstrated an optical fiber biosensor for the determination of intracellular guanosine 3', 5'-cyclic monophosphate (cGMP), which is an important second messenger for signal transduction within cells [149]. The target molecule was detected through the specific interaction with cGMP antiserum covalently attached to cystamine functionalized sAuNPs; a LOD in buffer was determined to be 0.1 nM.

Lactose intolerance-related DNA was targeted by Soares *et al.*, who detected synthetic 50mer targets as well as 350mer PCR products extracted from saliva samples via hybridization with thiolated probes immobilized on the Au nanotriangles [125]. Influence of mutation position on hybridization efficiency was studied as well.

B. Molecular Biology Applications

The use of plasmonic biosensors in molecular biology has a long and rich history. For more than two decades SPR biosensor technology has been a pivotal tool for real-time investigation of molecular interactions, and has led to numerous discoveries and new developments: to date numbering in the thousands of publications [282], [283]. Although biosensors based on plasmonic nanostructures have been used for the study of biomolecules to much lesser extent, there are a number of recent publications that illustrate potential they hold for this field.

Conformational changes of the protein calmodulin were investigated by Hall *et al.* [150]. Calmodulin is an intracellular protein whose activity is regulated by the concentration of intracellular calcium. In this work, a recombinant protein construct of calmodulin (fused to a cutinase) was immobilized onto Ag nanoprisms via a phosphonate-terminated SAM. The conformational changes of calmodulin were induced by increased the concentration of calcium; the protein was forced to return to its original conformation by adding of a calcium chelating agent.

Another study of conformational states and binding affinity of biomolecules was reported by Cao *et al.* [284], who used U-shaped Au split-ring resonators functionalized with thiol-terminated ssDNA, which in the presence of monovalent ions folds into four-stranded G-quadruplexes. These G-quadruplexes were further exploited as aptamer-receptors for the specific binding of an arginine-glycine-glycine domain (RGG_9 peptide) of protein nucleolin, which is overexpressed in human cancer cells. The K^+-induced G-quadruplex formation and subsequent binding of RGG_9 peptide were observed in buffer; results were confirmed by surface enhanced Raman spectroscopy.

Investigation of the molecular recognition of sugar residues by lectin Concavalin A (ConA) in a polymer brush was performed by Kitano *et al.* [285]. The interaction between carbohydrate and lectin plays an important role in many biological processes, including cellular recognition, inflammation, signal transduction, cell adhesion, and cancer cell metastasis. In this work, a glycopolymer with many pendant mannose residues was exploited as a functional layer with sugar receptors deposited on a colloidal Au-coated glass substrate. They investigated the interaction of ConA with various modifications of the glycopolymer. Kinetic parameters of the interaction were determined, revealing the influence of the so-called cluster effect (multipoint cooperative binding of ConA in glycopolymer) on the association constant of ConA. In another study, Bellapardona *et al.* investigated the interaction between ConA and D-(+)-mannose [7]. Mannose was modified with a PEG-thiol linker and attached to the surface of AuNPs via chemisorption. The kinetic parameters of the interaction were determined in experiments employing a flow-through microfluidic system [Fig. 9(a)] and were found comparable with a previously published work [285]. The ability of the tetrameric ConA to bind four mannose ligands was exploited for the subsequent

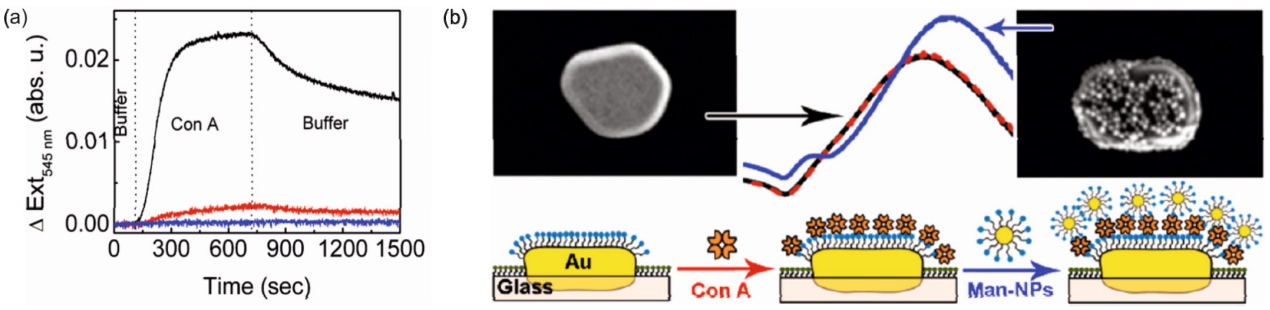

Fig. 9. *(a) ConA association and dissociation kinetics and determination of the binding affinity of ConA to a mannose. (b) Assay principle, UV-vis spectra, and HRSEM images corresponding to the binding of mannose-coated Au nanoparticles to ConA. Adapted with permission from [7]. Copyright 2012 ACS Publication.*

binding of mannose-functionalized AuNPs, providing both direct visualization of ConA binding as well as an enhancement of the sensor response [Fig. 9(b)].

An analysis of the interactions between low molecular weight aminoglycoside (AMG) antibiotics and RNA was presented by Frolov *et al.* [286]. AMG antibiotics specifically bind to the prokaryotic ribosomal RNA decoding region and interfere with protein translation, ultimately resulting in bacterial cell death. In this study, neomycin B, a highly potent AMG antibiotic, was selected as a target for screening with several RNA sequences. A PEG-thiol modified neomycin B was immobilized to the Au nanoislands and the impact of specific base substitutions in RNA constructs on the affinity and selectivity of the binding was studied.

The molecular interaction between nucleic acids and proteins was investigated by Song *et al.* [287]. An SP6 promoter (22mer DNA) and an SP6 RNA polymerase were employed to monitor sequence-specific binding of the polymerase to the DNA substrate and its three variants (having different single-point mutations). Each thiolated DNA substrate was attached to the surface of the AuNPs in a mixture with hydroxyl-terminated alkanthiols. A kinetic analysis demonstrated the effect of single-point mutations on the SP6–RNA polymerase binding.

Study of proteolytic activity of membrane type 1 matrix metalloproteinase (MT1–MMP) was performed by Hong *et al.* [288]. This metalloproteinase is involved in the proliferation and metastasis of cancer cells and may serve as an indicator of cancer invasion. In this work, dopamine-tagged MT1–MMP-specific cleavable peptide was immobilized to PEG functionalized Au nanorods via Au-catechol interaction. The MT1–MMP catalytic activity was observed as a blue shift in LSPR spectra and quantified both in buffer and cell lysate.

VIII. CONCLUDING REMARKS

Recent advances in both plasmonics and nanofabrication technologies have opened multiple avenues of research into plasmonic biosensors. Various plasmonic modes [e.g., localized surface plasmons (LSPs), coupled LSP–PSP modes, surface lattice resonances, Fano resonances] supported by metal or metal–dielectric nanostructures have been introduced to sensing and demonstrated to offer potentially attractive features (e.g., controlled localization of EM field at nanoscale). Plasmonic nanostructures have been utilized with a multitude of optical systems, whereby plasmonic modes can be excited using direct illumination, attenuated total reflection, diffractive coupling, or coupling with modes of an optical waveguide and interrogated by measuring various characteristics of light (e.g., wavelength, intensity, phase) coupled to these plasmonic modes. The design of optical platforms for plasmonic biosensors has been driven not only by the properties of the respective plasmonic nanostructures, but also by the targeted applications, which have ranged from laboratory systems for highly sensitive measurements on an individual plasmonic nanoparticle to robust portable devices for the detection of biomolecular analytes in the field.

The performance of a plasmonic biosensor can be described by an array of characteristics; however, a lack of standardization, combined with differences in protocols to establish such characteristics, makes a fair comparison of the different configurations of plasmonic biosensors (or likewise, a comparison with other types of optical affinity biosensors) rather difficult. Although performance characteristics, such as the bulk refractive index sensitivity, figure of merit, and resolution are widely used in the plasmonic sensing community, their validity is limited mainly to an optical system of a biosensor and thus each needs to be interpreted with caution (e.g., when comparing biosensors employing plasmonic modes with a different degree of field localization). In optical affinity biosensors, the ability to resolve small analyte-induced changes in the refractive index, often taking place within a distance smaller than the decay length of a plasmonic mode, is of key importance. In this respect, optical sensors based on plasmonic nanostructures have been shown to offer a level of performance comparable to their counterparts employing PSPs on continuous metal films (SPR biosensors). Nevertheless, the reduction of surface area and interrogation volume—due to the use of more localized plasmonic modes inherent to nanostructures—is an attractive feature, providing several interesting possibilities for future applications of biosensors based on plasmonic nanostructures that remain out of reach of the limits offered by conventional SPR biosensors (e.g., investigation of single-molecule events). Often the best way to characterize the performance of a plasmonic biosensor (or compare it to other types of biosensors) is through its ability to detect low concentrations of a target analyte, which is typically expressed in terms of the LOD; however, it needs to be kept in mind that the LOD of a plasmonic biosensor is a product of a complex interplay of several functional biosensor components—including the plasmonic nanostructure, optical platform, microfluidic system, and functional coating—and, furthermore, may be strongly affected by the specifics of a targeted application (i.e., sample properties).

To date, optical biosensors based on plasmonic nanostructures have been used to detect a broad variety of analytes, ranging from small chemicals, through proteins and nucleic acids, to bacterial and viral pathogens. Most attention has been given to the development of plasmonic biosensors for the detection of analytes related to medical diagnostics, especially cancer biomarkers. It should not go unnoticed, however, that the bulk of reported experiments have been focused on proof-of-concept experiments where detection was performed in buffers rather than in medically relevant samples, such as bodily fluids or tissue extracts. While LODs as low as 10^{-5} ng/ml have been reported for the detection of biomarkers in buffers, LODs achieved in blood serum remain much

higher, typically on the order of 1–10 ng/ml. While such performance may be sufficient for some applications, an improvement in the detection capabilities in complex samples would substantially expand the range of possible applications of plasmonic biosensors. In spite of recent advancements in the development of low-fouling functional coatings, the nonspecific adsorption of nontarget molecules from a sample matrix remains the main challenge that needs to be overcome to enable plasmonic biosensors to enter routine analytical practice.

Acknowledgment

The authors would like to thank Dr. N. S. Lynn Jr. from the Institute of Photonics and Electronics for valuable comments and suggestions.

REFERENCES

[1] G. Cappi *et al.*, "Label-free detection of tobramycin in serum by transmission-localized surface plasmon resonance," *Anal. Chem.*, vol. 87, pp. 5278–5285, May 2015.

[2] B.-R. Oh *et al.*, "Integrated nanoplasmonic sensing for cellular functional immunoanalysis using human blood," *ACS Nano*, vol. 8, pp. 2667–2676, Mar. 2014.

[3] M. Svedendahl, R. Verre, and M. Käll, "Refractometric biosensing based on optical phase flips in sparse and short-range-ordered nanoplasmonic layers," *Light Sci. Appl.*, vol. 3, p. e220, Nov. 2014.

[4] M. A. Otte *et al.*, "Identification of the optimal spectral region for plasmonic and nanoplasmonic sensing," *ACS Nano*, vol. 4, pp. 349–357, Jan. 2010.

[5] C. Huang *et al.*, "An on-chip localized surface plasmon resonance-based biosensor for label-free monitoring of antigen–antibody reaction," *Microelectron. Eng.*, vol. 86, pp. 2437–2441, Dec. 2009.

[6] M. A. Otte *et al.*, "Improved biosensing capability with novel suspended nanodisks," *J. Phys. Chem. C*, vol. 115, pp. 5344–5351, Apr. 2011.

[7] G. Bellapadrona *et al.*, "Optimization of localized surface plasmon resonance transducers for studying carbohydrate–protein interactions," *Anal. Chem.*, vol. 84, pp. 232–240, Jan. 2012.

[8] B. Gallinet and O. J. F. Martin, "Refractive index sensing with subradiant modes: A framework to reduce losses in plasmonic nanostructures," *ACS Nano*, vol. 7, pp. 6978–6987, Aug. 2013.

[9] S. S. Acimovic *et al.*, "LSPR chip for parallel, rapid, and sensitive detection of cancer markers in serum," *Nano Lett.*, vol. 14, pp. 2636–2641, May 2014.

[10] L. Malic, K. Morton, L. Clime, and T. Veres, "All-thermoplastic nanoplasmonic microfluidic device for transmission SPR biosensing," *Lab Chip*, vol. 13, pp. 798–810, Mar. 2013.

[11] M. Fleischmann, P. J. Hendra, and A. J. McQuillan, "Raman spectra of pyridine adsorbed at a silver electrode," *Chem. Phys. Lett.*, vol. 26, no. 2, pp. 163–166, 1974.

[12] J. Homola, *Surface Plasmon Resonance Based Sensors*. New York, NY, USA:Springer-Verlag, 2006.

[13] H. Jiang *et al.*, "A biosensor based on periodic arrays of gold nanodisks under normal transmission," *Sens. Actuators A, Phys.*, vol. 189, pp. 474–480, Jan. 2013.

[14] A. E. Cetin *et al.*, "Handheld high-throughput plasmonic biosensor using computational on-chip imaging," *Light, Sci. Appl.*, vol. 3, p. e122, Jan. 2014.

[15] A.-P. Blanchard-Dionne, L. Guyot, S. Patskovsky, R. Gordon, and M. Meunier, "Intensity based surface plasmon resonance sensor using a nanohole rectangular array," *Opt. Exp.*, vol. 19, pp. 15041–15046, Aug. 2011.

[16] S. Chen, M. Svedendahl, M. Käll, L. Gunnarsson, and A. Dmitriev, "Ultrahigh sensitivity made simple: Nanoplasmonic label-free biosensing with an extremely low limit-of-detection for bacterial and cancer diagnostics," *Nanotechnology*, vol. 20, p. 434015, Oct. 2009.

[17] D. L. Jeanmaire and R. P. Van Duyne, "Surface Raman spectroelectrochemistry: Part I. Heterocyclic, aromatic, and aliphatic amines adsorbed on the anodized silver electrode," *J. Electroanal. Chem. Interfacial Electrochem.*, vol. 84, pp. 1–20, Nov. 1977.

[18] F. Eftekhari *et al.*, "Nanoholes as nanochannels: Flow-through plasmonic sensing," *Anal. Chem.*, vol. 81, pp. 4308–4311, Jun. 2009.

[19] P. Jia, H. Jiang, J. Sabarinathan, and J. Yang, "Plasmonic nanohole array sensors fabricated by template transfer with improved optical performance," *Nanotechnology*, vol. 24, p. 195501, May 2013.

[20] S. H. Lee, N. C. Lindquist, N. J. Wittenberg, L. R. Jordan, and S.-H. Oh, "Real-time full-spectral imaging and affinity measurements from 50 microfluidic channels using nanohole surface plasmon resonance," *Lab Chip*, vol. 12, no. 20, pp. 3882–3890, 2012.

[21] H. Im, J. N. Sutherland, J. A. Maynard, and S.-H. Oh, "Nanohole-based surface plasmon resonance instruments with improved spectral resolution quantify a broad range of antibody-ligand binding kinetics," *Anal. Chem.*, vol. 84, pp. 1941–1947, Feb. 2012.

[22] H.-H. Jeong *et al.*, "Real-time label-free immunoassay of interferon-gamma and prostate-specific antigen using a fiber-optic localized surface plasmon resonance sensor," *Biosens. Bioelectron.*, vol. 39, pp. 346–351, Jan. 2013.

[23] B. Liedberg, C. Nylander, and I. Lundsrom, "Surface-plasmon resonance for gas-detection and biosensing," *Sens. Actuators*, vol. 4, pp. 229–304.

[24] P. L. Truong, C. Cao, S. Park, M. Kim, and S. J. Sim, "A new method for non-labeling attomolar detection of diseases based on an individual gold nanorod immunosensor," *Lab Chip*, vol. 11, no. 15, pp. 2591–2597, 2011.

[25] C. Escobedo, A. G. Brolo, R. Gordon, and D. Sinton, "Optofluidic concentration: Plasmonic nanostructure as concentrator and sensor," *Nano Lett.*, vol. 12, pp. 1592–1596, Mar. 2012.

[26] E. Martinsson *et al.*, "Local refractive index sensing based on edge gold-coated silver nanoprisms," *J. Phys. Chem. C*, vol. 117, pp. 23148–23154, Nov. 2013.

[27] G. K. Joshi *et al.*, "Designing efficient localized surface plasmon resonance-based sensing platforms: Optimization of sensor response by controlling the edge length of gold nanoprisms," *J. Phys. Chem. C*, vol. 116, pp. 20990–21000, Oct. 2012.

[28] G. K. Joshi, P. J. McClory, S. Dolai, and R. Sardar, "Improved localized surface plasmon resonance biosensing sensitivity based on chemically-synthesized gold nanoprisms as plasmonic transducers," *J. Mater. Chem.*, vol. 22, no. 3, pp. 923–931, 2012.

[29] G. A. C. Tellez, S. Hassan, R. N. Tait, P. Berini, and R. Gordon, "Atomically flat symmetric elliptical nanohole arrays in a gold film for ultrasensitive refractive index sensing," *Lab Chip*, vol. 13, no. 13, pp. 2541–2546, 2013.

[30] C. H. Chen *et al.*, "Novel D-type fiber optic localized plasmon resonance sensor realized by femtosecond laser engraving," *J. Laser Micro Nanoeng.*, vol. 5, pp. 1–5, Feb. 2010.

[31] C.-T. Huang *et al.*, "A novel design of grooved fibers for fiber-optic localized plasmon resonance biosensors," *Sensors*, vol. 9, pp. 6456–6470, Aug. 2009.

[32] G. Liang *et al.*, "Plasma enhanced label-free immunoassay for alpha-fetoprotein based on a U-bend fiber-optic LSPR biosensor," *RSC Adv.*, vol. 5, no. 31, pp. 23990–23998, 2015.

[33] S. K. Dondapati *et al.*, "Label-free biosensing based on single gold nanostars as plasmonic transducers," *ACS Nano*, vol. 4, pp. 6318–6322, Nov. 2010.

[34] J. Homola, "Surface plasmon resonance sensors for detection of chemical and biological species," *Chem. Rev.*, vol. 108, no. 2, pp. 462–493, Feb. 2008.

[35] V. V. R. Sai, T. Kundu, and S. Mukherji, "Novel U-bent fiber optic probe for localized surface plasmon resonance based biosensor," *Biosens. Bioelectron.*, vol. 24, no. 9, pp. 2804–2809, May 2009.

[36] M. R. Jones, K. D. Osberg, R. J. Macfarlane, M. R. Langille, and C. A. Mirkin, "Templated techniques for the synthesis and assembly of plasmonic nanostructures," *Chem. Rev.* , vol. 111, pp. 3736–3827, Jun. 2011.

[37] A. Biswas *et al.*, "Advances in top–down and bottom–up surface nanofabrication: Techniques, applications & future prospects," *Adv. Colloid Interface Sci.*, vol. 170, pp. 2–27, Jan. 2012.

[38] H.-D. Yu, M. D. Regulacio, E. Ye, and M.-Y. Han, "Chemical routes to top-down nanofabrication," *Chem. Soc. Rev.*, vol. 42, no. 14, pp. 6006–6018, 2013.

[39] N. Guillot and M. L. de la Chapelle, "Lithographied nanostructures as nanosensors," *J. Nanophoton.*, vol. 6, p. 064506, Sep. 2012.

[40] N. C. Lindquist, P. Nagpal, K. M. McPeak, D. J. Norris, and S.-H. Oh, "Engineering metallic nanostructures for plasmonics and nanophotonics," *Rep. Prog. Phys.*, vol. 75, p. 036501, Mar. 2012.

[41] C.-H. Chen *et al.*, "Novel U-shape gold nanoparticles-modified optical fiber for localized plasmon resonance chemical sensing," *Microsyst. Technol.*, vol. 16, pp. 1207–1214, Jul. 2010.

[42] T. V. Shahbazyan and M. I. Stockman, Eds., "Plasmonics: Theory and applications preface," in *Plasmonics: Theory and Applications*, vol. 15. 2013, pp. 5–6.

[43] M. I. Stockman, "Nanoplasmonics: Past, present, and glimpse into future," *Opt. Exp.*, vol. 19, pp. 22029–22106, Oct. 2011.

[44] A. B. Dahlin, *Plasmonic Biosensors: An Integrated View of Refractometric Detection*, vol. 4. Amsterdam, The Netherlands: IOS Press BV, 2012.

[45] A. Dmitriev, *Nanoplasmonic Sensors*. New York, NY, USA: Springer-Verlag, 2012.

[46] Y.-T. Long and C. Jing, *Localized Surface Plasmon Resonance Based Nanobiosensors*. Heidelberg, Germany: Springer, 2014.

[47] W. Li *et al.*, "Antibody modified gold nano-mushroom arrays for rapid detection of alpha-fetoprotein," *Biosens. Bioelectron.*, vol. 68, pp. 468–474, Jun. 2015.

[48] K. M. Mayer and J. H. Hafner, "Localized surface plasmon resonance sensors," *Chem. Rev.*, vol. 111, no. 6, pp. 3828–3857, Jun. 2011.

[49] M.-C. Estevez, M. A. Otte, B. Sepulveda, and L. M. Lechuga, "Trends and challenges of refractometric nanoplasmonic biosensors: A review," *Anal. Chim. Acta*, vol. 806, pp. 55–73, Jan. 2014.

[50] E. Petryayeva and U. J. Krull, "Localized surface plasmon resonance: Nanostructures, bioassays and biosensing—A review," *Anal. Chim. Acta*, vol. 706, pp. 8–24, Nov. 2011.

[51] A. G. Brolo, "Plasmonics for future biosensors," *Nature Photon.*, vol. 6, no. 11, pp. 709–713, Nov. 2012.

[52] A. B. Dahlin, "Sensing applications based on plasmonic nanopores: The hole story," *Analyst*, vol. 140, no. 14, pp. 4748–4759, 2015.

[53] O. Kedem, A. Vaskevich, and I. Rubinstein, "Critical issues in localized plasmon sensing," *J. Phys. Chem. C*, vol. 118, pp. 8227–8244, Apr. 2014.

[54] B. Sepúlveda, P. C. Angelomé, L. M. Lechuga, and L. M. Liz-Marzán, "LSPR-based nanobiosensors," *Nano Today*, vol. 4, no. 3, pp. 244–251, Jun. 2009.

[55] S. Szunerits and R. Boukherroub, "Sensing using localised surface plasmon resonance sensors," *Chem. Commun.*, vol. 48, no. 72, pp. 8999–9010, 2012.

[56] E. Petryayeva and U. J. Krull, "Localized surface plasmon resonance: Nanostructures, bioassays and biosensing—A review," *Anal. Chim. Acta*, vol. 706, pp. 8–24, Nov. 2011.

[57] M. I. Stockman, "Nanoplasmonic sensing and detection," *Science*, vol. 348, pp. 287–288, Apr. 2015.

[58] C. Valsecchi and A. G. Brolo, "Periodic metallic nanostructures as plasmonic chemical sensors," *Langmuir*, vol. 29, no. 19, pp. 5638–5649, May 2013.

[59] C. Huang, J. Ye, S. Wang, T. Stakenborg, and L. Lagae, "Gold nanoring as a sensitive plasmonic biosensor for on-chip DNA detection," *Appl. Phys. Lett.*, vol. 100, p. 173114, Apr. 2012.

[60] P. Singh, "SPR biosensors: Historical perspectives and current challenges," *Sens. Actuators B, Chem.*, vol. 229, pp. 110–130, Jun. 2016.

[61] C. Situ, J. Buijs, M. H. Mooney, and C. T. Elliott, "Advances in surface plasmon resonance biosensor technology towards high-throughput, food-safety analysis," *TrAC Trends Anal. Chem.*, vol. 29, pp. 1305–1315, Dec. 2010.

[62] C. L. Wong and M. Olivo, "Surface plasmon resonance imaging sensors: A review," *Plasmonics*, vol. 9, pp. 809–824, Aug. 2014.

[63] H. H. Nguyen, J. Park, S. Kang, and M. Kim, "Surface plasmon resonance: A versatile technique for biosensor applications," *Sensors*, vol. 15, pp. 10481–10510, May 2015.

[64] X. Wang, S. Zhan, Z. Huang, and X. Hong, "Review: Advances and applications of surface plasmon resonance biosensing instrumentation," *Instrum. Sci. Technol.*, vol. 41, pp. 574–607, Nov. 2013.

[65] K. Saha, S. S. Agasti, C. Kim, X. Li, and V. M. Rotello, "Gold nanoparticles in chemical and biological sensing," *Chem. Rev.*, vol. 112, no. 5, pp. 2739–2779, May 2012.

[66] S. Zeng *et al.*, "A review on functionalized gold nanoparticles for biosensing applications," *Plasmonics*, vol. 6, pp. 491–506, Sep. 2011.

[67] S. Lee, K. M. Mayer, and J. H. Hafner, "Improved localized surface plasmon resonance immunoassay with gold bipyramid substrates," *Anal. Chem.*, vol. 81, no. 11, pp. 4450–4455, Jun. 2009.

[68] J. Yuan, R. Duan, H. Yang, X. Luo, and M. Xi, "Detection of serum human epididymis secretory protein 4 in patients with ovarian cancer using a label-free biosensor based on localized surface plasmon resonance," *Int. J. Nanomed.*, vol. 7, pp. 2921–2928, 2012.

[69] Y.-C. Huang *et al.*, "Quantification of tumor necrosis factor-α and matrix metalloproteinases-3 in synovial fluid by a fiber-optic particle plasmon resonance sensor," *Analyst*, vol. 138, no. 16, pp. 4599–4606, 2013.

[70] F. J. Rodríguez-Fortuño *et al.*, "Highly-sensitive chemical detection in the infrared regime using plasmonic gold nanocrosses," *Appl. Phys. Lett.*, vol. 98, p. 133118, Mar. 2011.

[71] Q. Zhao *et al.*, "A reusable localized surface plasmon resonance biosensor for quantitative detection of serum squamous cell carcinoma antigen in cervical cancer patients based on silver nanoparticles array," *Int. J. Nanomed.*, vol. 9, pp. 1097–1104, Feb. 2014.

[72] S. A. Maier, *Plasmonics: Fundamentals and Applications*. New York, NY, USA:Springer-Verlag, 2007.

[73] H.-Y. Lin, C.-H. Huang, S.-H. Lu, I.-T. Kuo, and L.-K. Chau, "Direct detection of orchid viruses using nanorod-based fiber optic particle plasmon resonance immunosensor," *Biosens. Bioelectron.*, vol. 51, pp. 371–378, Jan. 2014.

[74] S. L. Dodson, C. Cao, H. Zaribafzadeh, S. Z. Li, and Q. H. Xiong, "Engineering plasmonic nanorod arrays for colon cancer marker detection," *Biosens. Bioelectron.*, vol. 63, pp. 472–477, Jan. 2015.

[75] C.-T. Li, H.-F. Chen, I.-W. Un, H.-C. Lee, and T.-J. Yen, "Study of optical phase transduction on localized surface plasmon resonance for ultrasensitive detection," *Opt. Exp.*, vol. 20, no. 3, pp. 3250–3260, Jan. 2012.

[76] S. J. Oldenburg, J. B. Jackson, S. L. Westcott, and N. J. Halas, "Infrared extinction properties of gold nanoshells," *Appl. Phys. Lett.*, vol. 75, no. 19, pp. 2897–2899, Nov. 1999.

[77] X. Ma, P. L. Truong, N. H. Anh, and S. J. Sim, "Single gold nanoplasmonic sensor for clinical cancer diagnosis based on specific interaction between nucleic acids and protein," *Biosens. Bioelectron.*, vol. 67, pp. 59–65, May 2015.

[78] A. H. Nguyen and S. J. Sim, "Nanoplasmonic biosensor: Detection and amplification of dual bio-signatures of circulating tumor DNA," *Biosens. Bioelectron.*, vol. 67, pp. 443–449, May 2015.

[79] J. Aizpurua *et al.*, "Optical properties of gold nanorings," *Phys. Rev. Lett.*, vol. 90, no. 5, p. 057401, Feb. 2003.

[80] Y. Zhan, D. Y. Lei, X. Li, and S. A. Maier, "Plasmonic Fano resonances in nanohole quadrumers for ultra-sensitive refractive index sensing," *Nanoscale*, vol. 6, no. 9, pp. 4705–4715, 2014.

[81] R. S. Moirangthem, M. T. Yaseen, P.-K. Wei, J.-Y. Cheng, and Y.-C. Chang, "Enhanced localized plasmonic detections using partially-embedded gold nanoparticles and ellipsometric measurements," *Biomed. Opt. Exp.*, vol. 3, no. 5, pp. 899–910, May 2012.

[82] A. H. Nguyen, X. Y. Ma, and S. J. Sim, "Gold nanostar based biosensor detects epigenetic alterations on promoter of real cells," *Biosens. Bioelectron.*, vol. 66, pp. 497–503, Apr. 2015.

[83] A. I. Aristov *et al.*, "Laser-ablative engineering of phase singularities in plasmonic metamaterial arrays for biosensing applications," *Appl. Phys. Lett.*, vol. 104, no. 7, p. 071101, Feb. 2014.

[84] H. J. Chen, L. Shao, Q. Li, and J. F. Wang, "Gold nanorods and their plasmonic properties," *Chem. Soc. Rev.*, vol. 42, no. 7, pp. 2679–2724, 2013.

[85] W. Kubo and S. Fujikawa, "Au double nanopillars with nanogap for plasmonic sensor," *Nano Lett.*, vol. 11, no. 1, pp. 8–15, Jan. 2011.

[86] R. Q. Duan, J. L. Yuan, H. Yang, X. G. Luo, and M. R. Xi, "Detection of p53 gene mutation by using a novel biosensor based on localized surface plasmon resonance," *Neoplasma*, vol. 59, no. 3, pp. 348–353, 2012.

[87] A. E. Çetin *et al.*, "Monopole antenna arrays for optical trapping, spectroscopy, and sensing," *Appl. Phys. Lett.*, vol. 98, no. 11, p. 111110, Mar. 2011.

[88] F. Inci *et al.*, "Nanoplasmonic quantitative detection of intact viruses from unprocessed whole blood," *Acs Nano*, vol. 7, no. 6, pp. 4733–4745 , Jun. 2013.

[89] L. Sherry, R. Jin, C. A. Mirkin, G. C. Schatz, and R. P. Van Duyne, "Localized surface plasmon resonance spectroscopy of single silver triangular nanoprisms," *Nano Lett.*, vol. 6, no. 9, pp. 2060–2065, Sep. 2006.

[90] Y. Shen *et al.*, "Plasmonic gold mushroom arrays with refractive index sensing figures of merit approaching the theoretical limit," *Nature Commun.*, vol. 4, Aug. 2013, Art. no. 2381.

[91] J.-H. Lee, B.-C. Kim, B.-K. Oh, and J.-W. Choi, "Highly sensitive localized surface plasmon resonance immunosensor for label-free detection of HIV-1," *Nanomed.-*

Nanotechnol., Biol. Med., vol. 9, no. 7, pp. 1018–1026, Oct. 2013.

[92] C. L. Nehl, H. W. Liao, and J. H. Hafner, "Optical properties of star-shaped gold nanoparticles," *Nano Lett.*, vol. 6, no. 4, pp. 683–688, Apr. 2006.

[93] N. Liu *et al.*, "Planar metamaterial analogue of electromagnetically induced transparency for plasmonic sensing," *Nano Lett.*, vol. 10, no. 4, pp. 1103–1107, Apr. 2010.

[94] S.-D. Liu, Z. Yang, R.-P. Liu, and X.-Y. Li, "High sensitivity localized surface plasmon resonance sensing using a double split nanoring cavity," *J. Phys. Chem. C*, vol. 115, no. 50, pp. 24469–24477, Dec. 2011.

[95] N. Liu, M. Mesch, T. Weiss, M. Hentschel, and H. Giessen, "Infrared perfect absorber and its application as plasmonic sensor," *Nano Lett.*, vol. 10, no. 7, pp. 2342–2348, Jul. 2010.

[96] B. Lahiri, A. Z. Khokhar, R. M. De La Rue, S. G. McMeekin, and N. P. Johnson, "Asymmetric split ring resonators for optical sensing of organic materials," *Opt. Exp.*, vol. 17, no. 2, pp. 1107–1115, Jan. 2009.

[97] J. P. Monteiro *et al.*, "Effect of periodicity on the performance of surface plasmon resonance sensors based on subwavelength nanohole arrays," *Sens. Actuators B, Chem.*, vol. 178, pp. 366–370, Mar. 2013.

[98] S. Zheng, D.-K. Kim, T. J. Park, S. J. Lee, and S. Y. Lee, "Label-free optical diagnosis of hepatitis B virus with genetically engineered fusion proteins," *Talanta*, vol. 82, no. 2, pp. 803–809, Jul. 2010.

[99] P. Offermans *et al.*, "Universal scaling of the figure of merit of plasmonic sensors," *ACS Nano*, vol. 5, no. 6, pp. 5151–5157, Jun. 2011.

[100] P. K. Jain and M. A. El-Sayed, "Plasmonic coupling in noble metal nanostructures," *Chem. Phys. Lett.*, vol. 487, nos. 4–6, pp. 153–164, Mar. 2010.

[101] A. A. Yanik *et al.*, "An optofluidic nanoplasmonic biosensor for direct detection of live viruses from biological media," *Nano Lett.*, vol. 10, no. 12, pp. 4962–4969, Dec. 2010.

[102] S. M. Yoo, D.-K. Kim, and S. Y. Lee, "Aptamer-functionalized localized surface plasmon resonance sensor for the multiplexed detection of different bacterial species," *Talanta*, vol. 132, pp. 112–117, Jan. 2015.

[103] B. Špačková and J. Homola, "Sensing properties of lattice resonances of 2-D metal nanoparticle arrays: An analytical model," *Opt. Exp.*, vol. 21, no. 22, pp. 27490–27502, Nov. 2013.

[104] A. A. Yanik *et al.*, "Seeing protein monolayers with naked eye through plasmonic Fano resonances," *Proc. Nat. Acad. Sci. USA*, vol. 108, no. 29, pp. 11784–11789, Jul. 2011.

[105] M. D. Malinsky, K. L. Kelly, G. C. Schatz, and R. P. Van Duyne, "Chain length dependence and sensing capabilities of the localized surface plasmon resonance of silver nanoparticles chemically modified with alkanethiol self-assembled monolayers," *J. Amer. Chem. Soc.*, vol. 123, no. 7, pp. 1471–1482, Feb. 21 2001.

[106] D. K. Kim *et al.*, "Plasmonic properties of the multispot copper-capped nanoparticle array chip and its application to optical biosensors for pathogen detection of multiplex DNAs," *Anal. Chem.*, vol. 83, no. 16, pp. 6215–6222, Aug. 2011.

[107] O. Kedem, A. B. Tesler, A. Vaskevich, and I. Rubinstein, "Sensitivity and optimization of localized surface plasmon resonance transducers," *Acs Nano*, vol. 5, no. 2, pp. 748–760, Feb. 2011.

[108] A. V. Kabashin *et al.*, "Plasmonic nanorod metamaterials for biosensing," *Nature Mater.*, vol. 8, no. 11, pp. 867–871, Nov. 2009.

[109] R. Bukasov, T. A. Ali, P. Nordlander, and J. S. Shumaker-Parry, "Probing the plasmonic near-field of gold nanocrescent antennas," *ACS Nano*, vol. 4, no. 11, pp. 6639–6650, Nov. 2010.

[110] Y.-T. Chang, Y.-C. Lai, C.-T. Li, C.-K. Chen, and T.-J. Yen, "A multi-functional plasmonic biosensor," *Opt. Exp.*, vol. 18, pp. 9561–9569, Apr. 2010.

[111] A. Degiron, H. J. Lezec, N. Yamamoto, and T. W. Ebbesen, "Optical transmission properties of a single subwavelength aperture in a real metal," *Opt. Commun.*, vol. 239, nos. 1–3, pp. 61–66, Sep. 2004.

[112] N. J. Halas, S. Lal, W. S. Chang, S. Link, and P. Nordlander, "Plasmons in strongly coupled metallic nanostructures," *Chem. Rev.*, vol. 111, no. 6, pp. 3913–3961, Jun. 2011.

[113] P. Y. Chen *et al.*, "Multiplex serum cytokine immunoassay using nanoplasmonic biosensor microarrays," *ACS Nano*, vol. 9, no. 4, pp. 4173–4181, Apr. 2015.

[114] S. S. Acimovic, M. P. Kreuzer, M. U. González, and R. Quidant, "Plasmon near-field coupling in metal dimers as a step toward single-molecule sensing," *ACS Nano*, vol. 3, no. 5, pp. 1231–1237, May 2009.

[115] M. Soler *et al.*, "Highly sensitive dendrimer-based nanoplasmonic biosensor for drug allergy diagnosis," *Biosens. Bioelectron.*, vol. 66, pp. 115–123, Apr. 2015.

[116] Y. Zhao, N. Engheta, and A. Alù, "Effects of shape and loading of optical nanoantennas on their sensitivity and radiation properties," *J. Opt. Soc. Amer. B, Opt. Phys.*, vol. 28, no. 5, pp. 1266–1274, May 2011.

[117] R. V. Olkhov, R. Parker, and A. M. Shaw, "Whole blood screening of antibodies using label-free nanoparticle biophotonic array platform," *Biosens. Bioelectron.*, vol. 36, pp. 1–5, Jun./Jul. 2012.

[118] Y. H. Jang *et al.*, "Configuration-controlled Au nanocluster arrays on inverse micelle nano-patterns: Versatile platforms for SERS and SPR sensors," *Nanoscale*, vol. 5, no. 24, pp. 12261–12271, 2013.

[119] J. B. Lassiter *et al.*, "Fano resonances in plasmonic nanoclusters: Geometrical and chemical tunability," *Nano Lett.*, vol. 10, no. 8, pp. 3184–3189, Aug. 2010.

[120] B. Yan, S. V. Boriskina, and B. M. Reinhard, "Optimizing gold nanoparticle cluster configurations (n (7) for array applications," *J. Phys. Chem. C*, vol. 115, no. 11, pp. 4578–4583, Mar. 2011.

[121] J. N. He, P. Ding, J. Q. Wang, C. Z. Fan, and E. J. Liang, "Double Fano-type resonances in heptamer-hole array transmission spectra with high refractive index sensing," *J. Modern Opt.*, vol. 62, no. 15, pp. 1241–1247 , 2015.

[122] T. Lai, Q. Hou, H. Yang, X. Luo, and M. Xi, "Clinical application of a novel sliver nanoparticles biosensor based on localized surface plasmon resonance for detecting the microalbuminuria," *Acta Biochim. Et Biophys. Sinica*, vol. 42, no. 11, pp. 787–792, Nov. 2010.

[123] F. Hao *et al.*, "Symmetry breaking in plasmonic nanocavities: Subradiant LSPR sensing and a tunable fano resonance," *Nano Lett.*, vol. 8, no. 11, pp. 3983–3988, Nov. 2008.

[124] S. Y. Yoo *et al.*, "Detection of the most common corneal dystrophies caused by BIGH3 gene point mutations using a multispot gold-capped nanoparticle array chip," *Anal. Chem.*, vol. 82, no. 4, pp. 1349–1357, Feb. 2010.

[125] L. Soares *et al.*, "Localized surface plasmon resonance (LSPR) biosensing using gold nanotriangles: Detection of DNA hybridization events at room temperature," *Analyst*, vol. 139, no. 19, pp. 4964–4973, 2014.

[126] S. P. Zhang, K. Bao, N. J. Halas, H. X. Xu, and P. Nordlander, "Substrate-induced fano resonances of a plasmonic nanocube: A route to increased-sensitivity localized surface plasmon resonance sensors revealed," *Nano Lett.*, vol. 11, no. 4, pp. 1657–1663, Apr. 2011.

[127] B. Luk *et al.*, "The Fano resonance in plasmonic nanostructures and metamaterials," *Nature Mater.*, vol. 9, pp. 707–715, Sep. 2010.

[128] B. Gallinet and O. J. F. Martin, "Influence of electromagnetic interactions on the line shape of plasmonic fano resonances," *ACS Nano*, vol. 5, no. 11, pp. 8999–9008, Nov. 2011.

[129] G. K. Joshi, M. A. Johnson, and R. Sardar, "Novel pH-responsive nanoplasmonic sensor: Controlling polymer structural change to modulate localized surface plasmon resonance response," *RSC Adv.*, vol. 4, no. 30, pp. 15807–15815, 2014.

[130] S. L. Zou, N. Janel, and G. C. Schatz, "Silver nanoparticle array structures that produce remarkably narrow plasmon lineshapes," *J. Chem. Phys.*, vol. 120, no. 23, pp. 10871–10875, Jun. 2004.

[131] F. J. G. de Abajo, "Colloquium: Light scattering by particle and hole arrays," *Rev. Modern Phys.*, vol. 79, no. 4, pp. 1267–1290, Oct./Dec. 2007.

[132] B. Auguié and W. L. Barnes, "Collective resonances in gold nanoparticle arrays," *Phys. Rev. Lett.*, vol. 101, no. 14, p. 143902, Oct. 2008.

[133] E. M. Hicks *et al.*, "Controlling plasmon line shapes through diffractive coupling in linear arrays of cylindrical nanoparticles fabricated by electron beam lithography," *Nano Lett.*, vol. 5, no. 6, pp. 1065–1070, Jun. 2005.

[134] Y. Wu, P. Dong, A. Deng, and J. Di, "Development of a label-free and reagentless plasmonic immunosensor for the detection of salbutamol," *Anal. Methods*, vol. 5, no. 19, pp. 5222–5226, 2013.

[135] Z. Yan, T. Hu, W. Guo, A. Deng, and J. Di, "A label-free immunosensor for determination of salbutamol based on localized surface plasmon resonance biosensing," *Bioprocess Biosyst. Eng.*, vol. 37, no. 4, pp. 651–657 , Apr. 2014.

[136] J. R. L. Guerreiro *et al.*, "Multifunctional biosensor based on localized surface plasmon resonance for monitoring small molecule–protein interaction," *Acs Nano*, vol. 8, no. 8, pp. 7958–7967, Aug. 2014.

[137] J. Ozhikandathil, S. Badilescu, and M. Packirisamy, "Gold nanoisland structures integrated in a lab-on-a-chip for plasmonic detection of bovine growth hormone," *J. Biomed. Opt.*, vol. 17, no. 7, p. 077001, Jul. 2012.

[138] S.-H. Chang, S. K. Gray, and G. C. Schatz, "Surface plasmon generation and light transmission by isolated nanoholes and arrays of nanoholes in thin metal films," *Opt. Exp.*, vol. 13, no. 8, pp. 3150–3165, Apr. 2005.

[139] T. Nagatsuka *et al.*, "Localized surface plasmon resonance detection of biological toxins using cell surface oligosaccharides on glyco chips," *ACS Appl. Mater. Interfaces*, vol. 5, no. 10, pp. 4173–4180, May 2013.

[140] F. Mazzotta *et al.*, "Influence of the evanescent field decay length on the sensitivity of plasmonic nanodisks and nanoholes," *ACS Photon.*, vol. 2, no. 2, pp. 256–262 , Feb. 2015.

[141] J.-H. Park *et al.*, "A regeneratable, label-free, localized surface plasmon resonance (LSPR) aptasensor for the detection of ochratoxin A," *Biosens. Bioelectron.*, vol. 59, pp. 321–327, Sep. 2014.

[142] T. W. Ebbesen, H. J. Lezec, H. F. Ghaemi, T. Thio, and P. A. Wolf, "Extraordinary optical transmission through sub-wavelength hole arrays," *Nature*, vol. 391, pp. 667–669, Feb. 1998.

[143] S. Y. Gao *et al.*, "Innovative platform for transmission localized surface plasmon transducers and its application in detecting heavy metal Pd(II)," *Anal. Chem.*, vol. 81, no. 18, pp. 7703–7712, Sep. 2009.

[144] H. Gao *et al.*, "Rayleigh anomaly-surface plasmon polariton resonances in palladium and gold subwavelength hole arrays," *Opt. Exp.*, vol. 17, no. 4, pp. 2334–2340, Feb. 2009.

[145] J.-F. Masson, M.-P. Murray-Méthot, and L. S. Live, "Nanohole arrays in chemical analysis: Manufacturing methods and applications," *Analyst*, vol. 135, no. 7, pp. 1483–1489, 2010.

[146] W. Zheng, H. C. Chiamori, G. L. Liu, L. W. Lin, and F. F. Chen, "Nanofabricated plasmonic nano-bio hybrid structures in biomedical detection," *Nanotechnol. Rev.*, vol. 1, pp. 213–233, Jun. 2012.

[147] J. Cao, T. Sun, and K. T. V. Grattan, "Gold nanorod-based localized surface plasmon resonance biosensors: A review," *Sens. Actuators B, Chem.*, vol. 195, pp. 332–351, May 2014.

[148] T. J. Lin and M. F. Chung, "Detection of cadmium by a fiber-optic biosensor based on localized surface plasmon resonance," *Biosens. Bioelectron.*, vol. 24, pp. 1213–1218, Jan. 2009.

[149] K. T. Huang, T. J. Lin, and M. H. Hsu, "Determination of cyclic GMP concentration using a gold nanoparticle-modified optical fiber," *Biosens. Bioelectron.*, vol. 26, pp. 11–15, Sep. 2010.

[150] W. P. Hall *et al.*, "A conformation- and ion-sensitive plasmonic biosensor," *Nano Lett.*, vol. 11, pp. 1098–1105, Mar. 2011.

[151] L. Guo *et al.*, "Enantioselective analysis of melagatran via an LSPR biosensor integrated with a microfluidic chip," *Lab Chip*, vol. 12, pp. 3901–3906, 2012.

[152] L. Guo *et al.*, "Discrimination of enantiomers based on LSPR biosensors fabricated with weak enantioselective and nonselective receptors," *Biosens. Bioelectron.*, vol. 47, pp. 199–205, Sep. 2013.

[153] M. Couture *et al.*, "Tuning the 3D plasmon field of nanohole arrays," *Nanoscale*, vol. 5, pp. 12399–12408, 2013.

[154] J. Li *et al.*, "Biosensing using diffractively coupled plasmonic crystals: The figure of merit revisited," *Adv. Opt. Mater.*, vol. 3, pp. 176–181, Feb. 2015.

[155] J. Li *et al.*, "Revisiting the surface sensitivity of nanoplasmonic biosensors," *ACS Photon.*, vol. 2, pp. 425–431, Mar. 2015.

[156] P. Kvasnička and J. Homola, "Optical sensors based on spectroscopy of localized surface plasmons on metallic nanoparticles: Sensitivity considerations," *Biointerphases*, vol. 3, pp. FD4–FD11, Sep. 2008.

[157] M. M. Miller and A. A. Lazarides, "Sensitivity of metal nanoparticle surface plasmon resonance to the dielectric environment," *J. Phys. Chem. B*, vol. 109, pp. 21556–21565, Nov. 2005.

[158] W. Y. Ma *et al.*, "Effects of vertex truncation of polyhedral nanostructures on localized surface plasmon resonance," *Opt. Exp.*, vol. 17, pp. 14967–14976, Aug. 2009.

[159] M. A. Mahmoud, M. Chamanzar, A. Adibi, and M. A. El-Sayed, "Effect of the dielectric constant of the surrounding medium and the substrate on the surface plasmon resonance spectrum and sensitivity factors of highly symmetric systems: Silver nanocubes," *J. Amer. Chem. Soc.*, vol. 134, pp. 6434–6442, Apr. 2012.

[160] B. Brian, B. Sepúlveda, Y. Alaverdyan, L. M. Lechuga, and M. Kall, "Sensitivity enhancement of nanoplasmonic sensors in low refractive index substrates," *Opt. Exp.*, vol. 17, pp. 2015–2023, Feb. 2009.

[161] X. Zhang *et al.*, "Elevated Ag nanohole arrays for high performance plasmonic sensors based on extraordinary optical transmission," *J. Mater. Chem.*, vol. 22, pp. 8903–8910, 2012.

[162] O. Kedem, A. Vaskevich, and I. Rubinstein, "Improved sensitivity of localized surface plasmon resonance transducers using reflection measurements," *J. Phys. Chem. Lett.*, vol. 2, pp. 1223–1226, May 2011.

[163] O. Kedem, A. Vaskevich, and I. Rubinstein, "Comparative assessment of the sensitivity of localized surface plasmon resonance transducers and interference-based Fabry–Pérot transducers," *Ann. Phys.*, vol. 524, pp. 713–722, Nov. 2012.

[164] B. Špačková *et al.*, "Ambiguous refractive index sensitivity of fano resonance on an array of gold nanoparticles," *Plasmonics*, vol. 9, pp. 729–735, Aug. 2014.

[165] J. Becker, A. Trügler, A. Jakab, U. Hohenester, and C. Sönnichsen, "The optimal aspect ratio of gold nanorods for plasmonic bio-sensing," *Plasmonics*, vol. 5, pp. 161–167, Jun. 2010.

[166] F. Hao, P. Nordlander, Y. Sonnefraud, P. Van Dorpe, and S. A. Maier, "Tunability of subradiant dipolar and Fano-type plasmon resonances in metallic ring/disk cavities: Implications for nanoscale optical sensing," *ACS Nano*, vol. 3, pp. 643–652, Mar. 2009.

[167] N. Verellen *et al.*, "Plasmon line shaping using nanocrosses for high sensitivity localized surface plasmon resonance sensing," *Nano Lett.*, vol. 11, no. 2, pp. 391–397, Feb. 2011.

[168] M. Piliarik, P. Kvasnička, N. Galler, J. R. Krenn, and J. Homola, "Local refractive index sensitivity of plasmonic nanoparticles," *Opt. Exp.*, vol. 19, pp. 9213–9220, May 2011.

[169] N.-H. Kim, W. K. Jung, and K. M. Byun, "Correlation analysis between plasmon field distribution and sensitivity enhancement in reflection- and transmission-type localized surface plasmon resonance biosensors," *Appl. Opt.*, vol. 50, pp. 4982–4988, Sep. 2011.

[170] A. J. Haes and R. P. Van Duyne, "A nanoscale optical biosensor: Sensitivity and selectivity of an approach based on the localized surface plasmon resonance spectroscopy of triangular silver nanoparticles," *J. Amer. Chem. Soc.*, vol. 124, pp. 10596–10604, Sep. 2002.

[171] E. Galopin *et al.*, "Short- and long-range sensing using plasmonic nanostrucures: Experimental and theoretical studies," *J. Phys. Chem. C*, vol. 113, pp. 15921–15927, Sep. 2009.

[172] W. A. Murray, J. R. Suckling, and W. L. Barnes, "Overlayers on silver nanotriangles: Field confinement and spectral position of localized surface plasmon resonances," *Nano Lett.*, vol. 6, pp. 1772–1777, Aug. 2006.

[173] O. Kedem, T. Sannomiya, A. Vaskevich, and I. Rubinstein, "Oscillatory behavior of the long-range response of localized surface plasmon resonance transducers," *J. Phys. Chem. C*, vol. 116, pp. 26865–26873, Dec. 2012.

[174] O. Saison-Francioso *et al.*, "Plasmonic nanoparticles array for high-sensitivity sensing: A theoretical investigation," *J. Phys. Chem. C*, vol. 116, pp. 17819–17827, Aug. 2012.

[175] A. M. Lopatynskyi, O. G. Lopatynska, L. J. Guo, and V. I. Chegel, "Localized surface plasmon resonance biosensor—Part I: Theoretical study of sensitivity—Extended Mie approach," *IEEE Sensors J.*, vol. 11, no. 2, pp. 361–369, Feb. 2011.

[176] M. Svedendahl, S. Chen, A. Dmitriev, and M. Käll, "Refractometric sensing using propagating versus localized surface plasmons: A direct comparison," *Nano Lett.*, vol. 9, pp. 4428–4433, Dec. 2009.

[177] M. Piliarik *et al.*, "High-resolution biosensor based on localized surface plasmons," *Opt. Exp.*, vol. 20, pp. 672–680, Jan. 2012.

[178] K. M. Byun, S. M. Jang, S. J. Kim, and D. Kim, "Effect of target localization on the sensitivity of a localized surface plasmon resonance biosensor based on subwavelength metallic nanostructures," *J. Opt. Soc. Amer. A, Opt. Image Sci. Vis.*, vol. 26, no. 4, pp. 1027–1034, Apr. 2009.

[179] Y. Gao, Q. Gan, and F. J. Bartoli, "Spatially selective plasmonic sensing using metallic nanoslit arrays," *IEEE J. Sel. Topics Quantum Electron.*, vol. 20, no. 3, May/Jun. 2014, Art. no. 6900306.

[180] J. Y. Lin, A. D. Stuparu, M. D. Huntington, M. Mrksich, and T. W. Odom, "Nanopatterned substrates increase surface sensitivity for real-time biosensing," *J. Phys. Chem. C*, vol. 117, pp. 5286–5292, Mar. 2013.

[181] J. Ferreira *et al.*, "Attomolar protein detection using in-hole surface plasmon resonance," *J. Amer. Chem. Soc.*, vol. 131, pp. 436–437, Jan. 2009.

[182] L. Feuz, M. P. Jonsson, and F. Höök, "Material-selective surface chemistry for nanoplasmonic sensors: Optimizing sensitivity and controlling binding to local hot spots," *Nano Lett.*, vol. 12, pp. 873–879, Feb. 2012.

[183] L. Feuz, P. Jönsson, M. P. Jonsson, and F. Höök, "Improving the limit of detection of nanoscale sensors by directed binding to high-sensitivity areas," *ACS Nano*, vol. 4, pp. 2167–2177, Apr. 2010.

[184] G. J. Nusz, A. C. Curry, S. M. Marinakos, A. Wax, and A. Chilkoti, "Rational selection of gold nanorod geometry for label-free plasmonic biosensors," *ACS Nano*, vol. 3, pp. 795–806, Apr. 2009.

[185] W. Zhang and O. J. F. Martin, "A universal law for plasmon resonance shift in biosensing," *ACS Photon.*, vol. 2, pp. 144–150, Jan. 2015.

[186] I. Ament, J. Prasad, A. Henkel, S. Schmachtel, and C. Sönnichsen, "Single unlabeled protein detection on individual plasmonic nanoparticles," *Nano Lett.*, vol. 12, pp. 1092–1095, Feb. 2012.

[187] P. Zijlstra, P. M. R. Paulo, and M. Orrit, "Optical detection of single non-absorbing molecules using the surface plasmon resonance of a gold nanorod," *Nature Nanotechnol.*, vol. 7, pp. 379–382, Jun. 2012.

[188] K. M. Mayer, F. Hao, S. Lee, P. Nordlander, and J. H. Hafner, "A single molecule immunoassay by localized surface plasmon resonance," *Nanotechnol.*, vol. 21, p. 255503, Jun. 2010.

[189] W.-S. Liao *et al.*, "Benchtop chemistry for the rapid prototyping of label-free biosensors: Transmission localized surface plasmon resonance platforms," *Biointerphases*, vol. 4, pp. 80–85, Dec. 2009.

[190] N. C. Lindquist, T. W. Johnson, J. Jose, L. M. Otto, and S. H. Oh, "Ultrasmooth metallic films with buried nanostructures for backside reflection-mode plasmonic biosensing," *Ann. Phys.*, vol. 524, pp. 687–696, Nov. 2012.

[191] K. Hedsten *et al.*, "Optical label-free nanoplasmonic biosensing using a vertical-cavity surface-emitting laser and charge-coupled device," *Anal. Chem.*, vol. 82, pp. 1535–1539, Feb. 2010.

[192] G. Cappi *et al.*, "Peak shift measurement of localized surface plasmon resonance by a portable electronic system," *Sens. Actuators B, Chem.*, vol. 176, pp. 225–231, Jan. 2013.

[193] P. J. R. Roche, S. Filion-Côté, M. C.-K. Cheung, V. P. Chodavarapu, and A. G. Kirk, "A camera phone localised surface plasmon biosensing platform towards low-cost label-free diagnostic testing," *J. Sensors*, vol. 2011, Sep. 2011, Art. no. 406425.

[194] L. S. Live *et al.*, "Angle-dependent resonance of localized and propagating surface plasmons in microhole arrays for enhanced biosensing," *Anal. Bioanal. Chem.*, vol. 404, pp. 2859–2868, Dec. 2012.

[195] V. G. Kravets *et al.*, "Singular phase nano-optics in plasmonic metamaterials for label-free single-molecule detection," *Nature Mater.*, vol. 12, pp. 304–309, Apr. 2013.

[196] A. B. Dahlin *et al.*, "High-resolution microspectroscopy of plasmonic nanostructures for miniaturized biosensing," *Anal. Chem.*, vol. 81, pp. 6572–6580, Aug. 2009.

[197] S. Kumar, N. J. Wittenberg, and S.-H. Oh, "Nanopore-induced spontaneous concentration for optofluidic sensing and particle assembly," *Anal. Chem.*, vol. 85, no. 2, pp. 971–977, Jan. 2013.

[198] H. Im, A. Lesuffleur, N. C. Lindquist, and S.-H. Oh, "Plasmonic nanoholes in a multichannel microarray format for parallel kinetic assays and differential sensing," *Anal. Chem.*, vol. 81, pp. 2854–2859, Apr. 2009.

[199] M. P. Raphael *et al.*, "Quantitative LSPR imaging for biosensing with single nanostructure resolution," *Biophys. J.*, vol. 104, pp. 30–36, Jan. 2013.

[200] H.-Y. Jin, D.-W. Li, N. Zhang, Z. Gu, and Y.-T. Long, "Analyzing carbohydrate–protein interaction based on single plasmonic nanoparticle by conventional dark field microscopy," *ACS Appl. Mater. Interfaces*, vol. 7, pp. 12249–12253, Jun. 2015.

[201] N. Jahr *et al.*, "Spectroscopy on single metallic nanoparticles using subwavelength apertures," *J. Phys. Chem. C*, vol. 117, pp. 7751–7756, Apr. 2013.

[202] M. Chamanzar, Z. Xia, S. Yegnanarayanan, and A. Adibi, "Hybrid integrated plasmonic-photonic waveguides for on-chip localized surface plasmon resonance (LSPR) sensing and spectroscopy," *Opt. Exp.*, vol. 21, no. 26, pp. 32086–32098, Dec. 2013.

[203] J. Cao, M. H. Tu, T. Sun, and K. T. V. Grattan, "Wavelength-based localized surface plasmon resonance optical fiber biosensor," *Sens. Actuators B, Chem.*, vol. 181, pp. 611–619, May 2013.

[204] M. Sanders, Y. Lin, J. Wei, T. Bono, and R. G. Lindquist, "An enhanced LSPR fiber-optic nanoprobe for ultrasensitive detection of protein biomarkers," *Biosens. Bioelectron.*, vol. 61, pp. 95–101, Nov. 2014.

[205] H.-H. Jeong, N. Erdene, S.-K. Lee, D.-H. Jeong, and J.-H. Park, "Fabrication of fiber-optic localized surface plasmon resonance sensor and its application to detect antibody-antigen reaction of interferon-gamma," *Opt. Eng.*, vol. 50, no. 12, p. 124405, Dec. 2011.

[206] Y. Lin, Y. Zou, and R. G. Lindquist, "A reflection-based localized surface plasmon resonance fiber-optic probe for biochemical sensing," *Biomed. Opt. Exp.*, vol. 2, pp. 478–484, Mar. 2011.

[207] A. R. Camara *et al.*, "Dengue immunoassay with an LSPR fiber optic sensor," *Opt. Exp.*, vol. 21, pp. 27023–27031, Nov. 2013.

[208] H. Lee, H.-J. Kim, J.-H. Park, D.-H. Jeong, and S.-K. Lee, "Effects of surface density and size of gold nanoparticles in a fiber-optic localized surface plasmon resonance sensor and its application to peptide detection," *Meas. Sci. Technol.*, vol. 21, p. 085805, Aug. 2010.

[209] N. Cennamo *et al.*, "Localized surface plasmon resonance with five-branched gold nanostars in a plastic optical fiber for bio-chemical sensor implementation," *Sensors*, vol. 13, pp. 14676–14686, Nov. 2013.

[210] J. Satija, N. S. Punjabi, V. V. R. Sai, and S. Mukherji, "Optimal design for U-bent fiber-optic LSPR sensor probes," *Plasmonics*, vol. 9, pp. 251–260, Apr. 2014.

[211] P. Jia and J. Yang, "A plasmonic optical fiber patterned by template transfer as a high-performance flexible nanoprobe for real-time biosensing," *Nanoscale*, vol. 6, pp. 8836–8843, Aug. 2014.

[212] Y. Lin, Y. Zou, Y. Mo, J. Guo, and R. G. Lindquist, "E-beam patterned gold nanodot arrays on optical fiber tips for localized surface plasmon resonance biochemical sensing," *Sensors*, vol. 10, pp. 9397–9406, Oct. 2010.

[213] B. Sciacca and T. M. Monro, "Dip biosensor based on localized surface plasmon resonance at the tip of an optical fiber," *Langmuir*, vol. 30, pp. 946–954, Jan. 2014.

[214] C. Caucheteur, T. Guo, and J. Albert, "Review of plasmonic fiber optic biochemical sensors: Improving the limit of detection," *Anal. Bioanal. Chem.*, vol. 407, no. 14, pp. 3883–3897, May 2015.

[215] J. Ozhikandathil and M. Packirisamy, "Nano-islands integrated evanescence-based lab-on-a-chip on silica-on-silicon and polydimethylsiloxane hybrid platform for detection of recombinant growth hormone," *Biomicrofluidics*, vol. 6, p. 046501, Dec. 2012.

[216] M. E. Stewart *et al.*, "Quantitative multispectral biosensing and 1D imaging using quasi-3D plasmonic crystals," *Proc. Nat. Acad. Sci. USA*, vol. 103, no. 6, pp. 17143–17148, Nov. 2006.

[217] K.-L. Lee and P.-K. Wei, "Enhancing surface plasmon detection using ultrasmall nanoslits and a multispectral integration method," *Small*, vol. 6, pp. 1900–1907, Sep. 2010.

[218] E.-H. Lin, W.-S. Tsai, K.-L. Lee, M.-C. Lee, and P.-K. Wei, "Enhancing detection sensitivity of metallic nanostructures by resonant coupling mode and spectral integration analysis," *Opt. Exp.*, vol. 22, pp. 19621–19632, Aug. 2014.

[219] K.-L. Lee *et al.*, "Improving surface plasmon detection in gold nanostructures using a multi-polarization spectral integration method," *Adv. Mater.*, vol. 24, pp. OP253–OP259, Sep. 2012.

[220] H. S. Leong and J. P. Guo, "Surface plasmon resonance in superperiodic metal nanoslits," *Opt. Lett.*, vol. 36, pp. 4764–4766, Dec. 2011.

[221] H. Guo and J. P. Guo, "Hybrid plasmon photonic crystal resonance grating for integrated spectrometer biosensor," *Opt. Lett.*, vol. 40, pp. 249–252, Jan. 2015.

[222] J. A. Ruemmele, W. P. Hall, L. K. Ruvuna, and R. P. van Duyne, "A localized surface plasmon resonance imaging instrument for multiplexed biosensing," *Anal. Chem.*, vol. 85, pp. 4560–4566, May 2013.

[223] H. Yoshikawa *et al.*, "Parallelized label-free detection of protein interactions using a hyper-spectral imaging system," *Anal. Methods*, vol. 7, no. 12, pp. 5157–5161, 2015.

[224] T. Y. Tseng, P. J. Lai, and K. B. Sung, "High-throughput detection of immobilized plasmonic nanoparticles by a hyperspectral imaging system based on Fourier transform spectrometry," *Opt. Exp.*, vol. 19, pp. 1291–1300, Jan. 2011.

[225] D. Zopf *et al.*, "Hyperspectral imaging of plasmon resonances in metallic nanoparticles," *Biosens. Bioelectr.*, vol. 81, pp. 287–293, Jul. 2016.

[226] K. H. Chen, J. Hobley, Y. L. Foo, and X. D. Su, "Wide-field single metal nanoparticle spectroscopy for high throughput localized surface plasmon resonance sensing," *Lab Chip*, vol. 11, pp. 1895–1901, 2011.

[227] X. Liu, Q. Zhang, Y. Tu, W. Zhao, and H. Gai, "Single gold nanoparticle localized surface plasmon resonance spectral imaging for quantifying binding constant of carbohydrate–protein interaction," *Anal. Chem.*, vol. 85, 2013.

[228] A. J. Thiel, A. G. Frutos, C. E. Jordan, R. M. Corn, and L. M. Smith, "In situ surface plasmon resonance imaging detection of DNA hybridization to oligonucleotide arrays on gold surfaces," *Anal. Chem.*, vol. 69, pp. 4948–4956, Dec. 1997.

[229] M. Piliarik, H. Vaisocherová, and J. Homola, "A new surface plasmon resonance sensor for high-throughput screening applications," *Biosens. Bioelectr.*, vol. 20, pp. 2104–2110, Apr. 2005.

[230] N. C. Lindquist, A. Lesuffleur, H. Im, and S. H. Oh, "Sub-micron resolution surface plasmon resonance imaging enabled by nanohole arrays with surrounding Bragg mirrors for enhanced sensitivity and isolation," *Lab Chip*, vol. 9, no. 3, pp. 382–387, 2009.

[231] Y. A. Wang *et al.*, "Transmissive nanohole arrays for massively-parallel optical biosensing," *ACS Photon.*, vol. 1, pp. 241–245, Mar. 2014.

[232] Y. H. Huang, H. P. Ho, S. K. Kong, and A. V. Kabashin, "Phase-sensitive surface plasmon resonance biosensors: Methodology, instrumentation and applications," *Ann. Der Physik*, vol. 524, pp. 637–662, Nov. 2012.

[233] Z. L. Cao, S. L. Wong, S. Y. Wu, H. P. Ho, and H. C. Ong, "High performing phase-based surface plasmon resonance sensing from metallic nanohole arrays," *Appl. Phys. Lett.*, vol. 104, no. 17, p. 171116, Apr. 2014.

[234] L. M. Otto, D. A. Mohr, T. W. Johnson, S. H. Oh, and N. C. Lindquist, "Polarization interferometry for real-time spectroscopic plasmonic sensing," *Nanoscale*, vol. 7, no. 9, pp. 4226–4233, 2015.

[235] A. R. Halpern, Y. Chen, R. M. Corn, and D. Kim, "Surface plasmon resonance phase imaging measurements of patterned monolayers and DNA adsorption onto microarrays," *Anal. Chem.*, vol. 83, pp. 2801–2806, Apr. 2011.

[236] M. Piliarik, L. Párová, and J. Homola, "High-throughput SPR sensor for food safety," *Biosens. Bioelectr.*, vol. 24, pp. 1399–1404, Jan. 2009.

[237] C. Huang *et al.*, "Localized surface plasmon resonance biosensor integrated with microfluidic chip," *Biomed. Microdevices*, vol. 11, no. 4, pp. 893–901, Nov. 2009.

[238] Y. Zhang *et al.*, "Towards a high-throughput label-free detection system combining localized-surface plasmon resonance and microfluidics," *Lab Chip*, vol. 12, no. 17, pp. 3012–3015, 2012.

[239] T. M. Squires, R. J. Messinger, and S. R. Manalis, "Making it stick: Convection, reaction and diffusion in surface-based biosensors," *Nature Biotechnol.*, vol. 26, pp. 417–426, Apr. 2008.

[240] N. S. Lynn, H. Šípová, P. Adam, and J. Homola, "Enhancement of affinity-based biosensors: Effect of sensing chamber geometry on sensitivity," *Lab Chip*, vol. 13, no. 7, pp. 1413–1421, 2013.

[241] A. A. Yanik, M. Huang, A. Artar, T. Y. Chang, and H. Altug, "Integrated nanoplasmonic-nanofluidic biosensors with targeted delivery of analytes," *Appl. Phys. Lett.*, vol. 96, no. 2, p. 021101, Jan. 2010.

[242] M. P. Jonsson, A. B. Dahlin, L. Feuz, S. Petronis, and F. Hook, "Locally functionalized short-range ordered nanoplasmonic pores for bioanalytical sensing," *Anal. Chem.*, vol. 82, pp. 2087–2094, Mar. 2010.

[243] I. A. Grimaldi, G. Testa, and R. Bernini, "Flow through ring resonator sensing platform," *RSC Adv.*, vol. 5, no. 86, pp. 70156–70162, 2015.

[244] M. Huang, B. C. Galarreta, A. E. Cetin, and H. Altug, "Actively transporting virus like analytes with optofluidics for rapid and ultrasensitive biodetection," *Lab Chip*, vol. 13, no. 24, pp. 4841–4847, 2013.

[245] A. Csaki *et al.*, "Nanoparticle layer deposition for plasmonic tuning of microstructured optical fibers," *Small*, vol. 6, pp. 2584–2589, Nov. 2010.

[246] A. Barik *et al.*, "Dielectrophoresis-enhanced plasmonic sensing with gold nanohole arrays," *Nano Lett.*, vol. 14, pp. 2006–2012, Apr. 2014.

[247] H. Vaisocherová, E. Brynda, and J. Homola, "Functionalizable low-fouling coatings for label-free biosensing in complex biological media: Advances and applications," *Anal. Bioanal. Chem.*, vol. 407, pp. 3927–3953, May 2015.

[248] F. Rusmini, Z. Y. Zhong, and J. Feijen, "Protein immobilization strategies for protein biochips," *Biomacromolecules*, vol. 8, pp. 1775–1789, Jun. 2007.

[249] R. G. Nuzzo and D. L. Allara, "Adsorption of bifunctional organic disulfides on gold surfaces," *J. Amer. Chem. Soc.*, vol. 105, no. 13, pp. 4481–4483, 1983.

[250] S. Balamurugan *et al.*, "Nanostructure shape effects on response of plasmonic aptamer sensors," *J. Molecular Recognit.*, vol. 26, pp. 402–407, Sep. 2013.

[251] L. H. Guo and D. H. Kim, "LSPR biomolecular assay with high sensitivity induced by aptamer-antigen-antibody sandwich complex," *Biosens. Bioelectr.*, vol. 31, pp. 567–570, Jan. 2012.

[252] C. Boozer, S. F. Chen, and S. Y. Jiang, "Controlling DNA orientation on mixed ssDNA/OEG SAMs," *Langmuir*, vol. 22, pp. 4694–4698, May 2006.

[253] P. Gong, C. Y. Lee, L. J. Gamble, D. G. Castner, and D. W. Grainger, "Hybridization behavior of mixed DNA/Alkylthiol monolayers on gold: Characterization by surface plasmon resonance and ^{32}P radiometric assay," *Anal. Chem.*, vol. 78, pp. 3326–3334, May 2006.

[254] M. Ogiso *et al.*, "Carbohydrate immobilized on a dendrimer-coated colloidal gold surface for fabrication of a lectin-sensing device based on localized surface plasmon resonance spectroscopy," *Biosens. Bioelectr.*, vol. 41, pp. 465–470, Mar. 2013.

[255] J. Y. Byun *et al.*, "The use of an engineered single chain variable fragment in a localized surface plasmon resonance method for analysis of the C-reactive protein," *Chem. Commun.*, vol. 49, no. 82, pp. 9497–9499, 2013.

[256] A. K. Trilling, J. Beekwilder, and H. Zuilhof, "Antibody orientation on biosensor surfaces: A minireview," *Analyst*, vol. 138, no. 6, pp. 1619–1627, 2013.

[257] K. Bonroy *et al.*, "Comparison of random and oriented immobilisation of antibody fragments on mixed self-assembled monolayers," *J. Immunol. Methods*, vol. 312, pp. 167–181, May 2006.

[258] T. J. Park, M. S. Hyun, H. J. Lee, S. Y. Lee, and S. Ko, "A self-assembled fusion protein-based surface plasmon resonance biosensor for rapid diagnosis of severe acute respiratory syndrome," *Talanta*, vol. 79, pp. 295–301, Jul. 2009.

[259] T. J. Park *et al.*, "Development of label-free optical diagnosis for sensitive detection of influenza virus with genetically engineered fusion protein," *Talanta*, vol. 89, pp. 246–252, Jan. 2012.

[260] S. R. Beeram and F. P. Zamborini, "Effect of protein binding coverage, location, and distance on the localized surface plasmon resonance response of purified au nanoplates grown directly on surfaces," *J. Phys. Chem. C*, vol. 115, pp. 7364–7371, Apr. 2011.

[261] P. L. Truong, B. W. Kim, and S. J. Sim, "Rational aspect ratio and suitable antibody coverage of gold nanorod for ultra-sensitive detection of a cancer biomarker," *Lab Chip*, vol. 12, no. 6, pp. 1102–1109, 2012.

[262] J. K. Bhattarai, A. Sharma, K. Fujikawa, A. V. Demchenko, and K. J. Stine, "Electrochemical synthesis of nanostructured gold film for the study of carbohydrate-lectin interactions using localized surface plasmon resonance spectroscopy," *Carbohydrate Res.* , vol. 405, pp. 55–65, Mar. 2015.

[263] H. Kitano *et al.*, "Binding of beta-secretase to a peptide inhibitor-carrying SAM," *Colloids Surfaces B, Biointerfaces*, vol. 78, pp. 155–162, Jul. 2010.

[264] E. Galopin *et al.*, "Amorphous silicon-carbon alloys for efficient localized surface plasmon resonance sensing," *Biosens. Bioelectr.*, vol. 25, pp. 1199–1203, Jan. 2010.

[265] L. Touahir *et al.*, "Plasmonic properties of silver nanostructures coated with an amorphous silicon–carbon alloy and their applications for sensitive sensing of DNA hybridization," *Analyst*, vol. 136, no. 9, pp. 1859–1866, 2011.

[266] J. Yamamichi *et al.*, "Surface chemical approach to single-step measurement of antibody in human serum using localized surface plasmon resonance biosensor on microtiter plate system," *Anal. Bioanal. Chem.*, vol. 406, pp. 4527–4533, Jul. 2014.

[267] J. Yamamichi *et al.*, "Single-step, label-free quantification of antibody in human serum for clinical applications based on localized surface plasmon resonance," *Nanomed., Nanotechnol. Biol. Med.*, vol. 7, no. 6, pp. 889–895, Dec. 2011.

[268] A. B. Turhan, D. Ataman, Y. Sen, M. Mutlu, andE. Özbay, "Nanofabrication and plasma polymerization assisted surface modification of a transducer based on localized surface plasmon resonance of gold nanostructure arrays for biosensor applications," *J. Nanophoton.*, vol. 6, no. 1, p. 061602, Jul. 2012.

[269] M. Soler *et al.*, "Direct detection of protein biomarkers in human fluids using site-specific antibody immobilization strategies," *Sensors*, vol. 14, no. 2, pp. 2239–2258, Feb. 2014.

[270] F.-Z. Tighilt *et al.*, "Localized surface plasmon resonance interfaces coated with poly[3-(pyrrolyl)carboxylic acid] for histidine-tagged peptide sensing," *Analyst*, vol. 136, no. 20, pp. 4211–4216, 2011.

[271] T. A. Gschneidtner, S. Chen, J. B. Christensen, M. Käll, and K. Moth-Poulsen, "Toward plasmonic biosensors functionalized by a photoinduced surface reaction," *J. Phys. Chem. C*, vol. 117, no. 28, pp. 14751–14758, Jul. 2013.

[272] S. R. Beeram and F. P. Zamborini, "Selective attachment of antibodies to the edges of gold nanostructures for enhanced localized surface plasmon resonance biosensing," *J. Amer. Chem. Soc.*, vol. 131, no. 33, pp. 11689–11691, Aug. 2009.

[273] M. J. Hostetler, A. C. Templeton, and R. W. Murray, "Dynamics of place-exchange reactions on monolayer-protected gold cluster molecules," *Langmuir*, vol. 15, no. 11, pp. 3782–3789, May 1999.

[274] A. Abbas, L. M. Tian, J. J. Morrissey, E. D. Kharasch, and S. Singamaneni, "Hot spot-localized artificial antibodies for label-free plasmonic biosensing," *Adv. Funct. Mater.*, vol. 23, no. 14, pp. 1789–1797, Apr. 2013.

[275] A. Abbas, L. Tian, R. Kattumenu, A. Halim, and S. Singamaneni, "Freezing the self-assembly process of gold nanocrystals," *Chem. Commun.*, vol. 48, no. 11, pp. 1677–1679, Feb. 2012.

[276] C. M. Galloway *et al.*, "Plasmon-assisted delivery of single nano-objects in an optical hot spot," *Nano Lett.*, vol. 13, no. 9, pp. 4299–4304, Sep. 2013.

[277] T. Špringer and J. Homola, "Biofunctionalized gold nanoparticles for SPR-biosensor-based detection of CEA in blood plasma," *Anal. Bioanal. Chem.*, vol. 404, no. 10, pp. 2869–2875, Dec. 2012.

[278] W. P. Hall, S. N. Ngatia, and R. P. Van Duyne, "LSPR biosensor signal enhancement using nanoparticle-antibody conjugates," *J. Phys. Chem. C*, vol. 115, no. 5, pp. 1410–1414, Feb. 2011.

[279] J. Spadavecchia *et al.*, "Approach for plasmonic based DNA sensing: Amplification of the wavelength shift and simultaneous detection of the plasmon modes of gold nanostructures," *Anal. Chem.*, vol. 85, no. 6, pp. 3288–3296, Mar. 2013.

[280] T. Schneider *et al.*, "Localized surface plasmon resonance (LSPR) study of DNA hybridization at single nanoparticle transducers," *J. Nanoparticle Res.*, vol. 15, p. 1531, Apr. 2013.

[281] T.-H. Lee *et al.*, "Signal amplification by enzymatic reaction in an immunosensor based on localized surface plasmon resonance (LSPR)," *Sensors*, vol. 10, no. 3, pp. 2045–2053, Mar. 2010.

[282] C. Boozer, G. Kim, S. Cong, H. W. Guan, and T. Londergan, "Looking towards label-free biomolecular interaction analysis in a high-throughput format: A review of new surface plasmon resonance technologies," *Current Opinion Biotechnol.*, vol. 17, pp. 400–405, Aug. 2006.

[283] R. L. Rich and D. G. Myszka, "Higher-throughput, label-free, real-time molecular interaction analysis," *Anal. Biochem.*, vol. 361, no. 1, pp. 1–6, Feb. 2007.

[284] C. Cao *et al.*, "Metamaterials-based label-free nanosensor for conformation and affinity biosensing," *ACS Nano*, vol. 7, no. 9, pp. 7583–7591, Sep. 2013.

[285] H. Kitano, Y. Takahashi, K. Mizukami, and K. Matsuura, "Kinetic study on the binding of lectin to mannose residues in a polymer brush," *Colloids Surf. B, Biointerfaces*, vol. 70, no. 1, pp. 91–97, Apr. 2009.

[286] L. Frolov *et al.*, "Direct observation of aminoglycoside–RNA binding by localized surface plasmon resonance spectroscopy," *Anal. Chem.*, vol. 85, no. 4, pp. 2200–2207, Feb. 2013.

[287] M. S. Song, S. P. Choi, J. Lee, Y. J. Kwon, and S. J. Sim, "Real-time, sensitive, and specific detection of promoter-polymerase interactions in gene transcription using a nanoplasmonic sensor," *Adv. Mater.*, vol. 25, no. 9, pp. 1265–1269, Mar. 2013.

[288] Y. Hong *et al.*, "Localized surface plasmon resonance based nanobiosensor for biomarker detection of invasive cancer cells," *J. Biomed. Opt.*, vol. 19, no. 5, p. 051202, May 2014.

ABOUT THE AUTHORS

Barbora Špačková received the M.S. and Ph.D. degrees in physical engineering from Czech Technical University, Prague, Czech Republic, in 2007 and in 2015, respectively.

Since 2007, she has been with the Institute of Photonics and Electronics, Czech Academy of Sciences, Prague, Czech Republic, where she became a Postdoctoral Fellow in 2015. Her research has been concerned with plasmonics and their application in optical sensors and biosensors.

Markéta Bocková received the M.S. degree in biochemistry from Charles University, Prague, Czech Republic, in 2009. She is currently working toward the Ph.D. degree in the Optical Biosensors Research Group, Institute of Photonics and Electronics, Czech Academy of Sciences, Prague, Czech Republic.

Her research interests include optical biosensors and functional coatings for detection of biomolecules and investigation of biomolecular interactions.

Piotr Wrobel received the M.S. and Ph.D. degrees in physics from the University of Warsaw, Warsaw, Poland, in 2007 and 2012, respectively.

Currently, he is a Postdoctoral Fellow at the Institute of Photonics and Electronics, Czech Academy of Sciences, Prague, Czech Republic. His current research interests include nanophotonics and plasmonic and their applications in biosensors.

Jiří Homola (Senior Member, IEEE) received the M.S. degree in physical engineering from the Czech Technical University, Prague, Czech Republic, in 1988 and the Ph.D. degree in electrical engineering and the D.Sc. degree in technical sciences from the Czech Academy of Sciences, Prague, Czech Republic, in 1993 and 2009, respectively.

From 1993 to 1997, he worked at the Institute of Photonics and Electronics, Czech Academy of Sciences, as a Research Scientist. In 1997-2002, he was with the Department of Electrical Engineering, University of Washington, Seattle, WA, USA, becoming a Research Associate Professor in 2001. From 2003 to 2012, he served as the Head of Photonics Division and Chairman of the Department of Optical Sensors, Institute of Photonics and Electronics, Czech Academy of Sciences. Currently, he is Director of the Institute of Photonics and Electronics, Czech Academy of Sciences. He also is Professor at Charles University, Prague, Czech Republic and Affiliate Professor at the University of Washington. His research interests are in (bio)photonics, plasmonics, optical sensors, and biosensors.

Prof. Homola is a Fellow of the International Society for Optics and Photonics (SPIE) and a member of the Learned Society of the Czech Republic.